NASA Contractor Report 189150

Coupled Structural/Thermal/Electromagnetic Analysis/Tailoring of Graded Composite Structures

First Annual Status Report

R.L. McKnight, P.C. Chen, L.T. Dame, H. Huang,
and M. Hartle
General Electric
Cincinnati, Ohio

April 1992

Prepared for
Lewis Research Center
Under Contract NAS3–24538

National Aeronautics and
Space Administration

FOREWORD

This report has been prepared to expedite early domestic dissemination of the information generated under the contract. The data and conclusions must be considered preliminary and subject to change as further progress is made on this program. This is a progress report covering the work done during the first 12 months of the contract; it is not a final report. The NASA Program Manager is Dr. C.C. Chamis.

ABSTRACT

Accomplishments are described for the first year effort of a 5-year program to develop a methodology for coupled structural/thermal/electromagnetic analysis/tailoring of graded composite structures. These accomplishments include: (1) the results of the selective literature survey; (2) 8-, 16-, and 20-noded isoparametric plate and shell elements; (3) large deformation structural analysis; (4) Eigenanalysis; (5) anisotropic heat transfer analysis; and (6) anisotropic electromagnetic analysis.

TABLE OF CONTENTS

LIST OF ILLUSTRATIONS

LIST OF TABLES

NOMENCLATURE

AEBG	-	Aircraft Engine Business Group
AID	-	Automatic Improvement of Design
$\vec{B}$	-	Magnetic Flux Density
C	-	Specific Heat
[C]	-	Damping Matrix
COLSOL	-	Linear Equations Solution Routine
COLSOV	-	Version of COLSOL for Heat Transfer
CSTEM	-	Coupled Structural/Thermal/Electromagnetic Analysis/ Tailoring of Graded Composite Structures
ESMOSS	-	Engine Structures Modeling Software System
FEM	-	Finite Element Method
$\{F_B\}$	-	Body Force Vector
$\{F_I\}$	-	Initial Strains Vector
$\{F_{NL}\}$	-	Nonlinear Strains Vector
$\{F_S\}$	-	Surface Tractions Vector
$G(x,y,z)$	-	Value of Function at Any Point (x,y,z)
$G(x_i,y_i,z_i)$	-	Value of Function at Node Point i
$\vec{H}$	-	Magnetic Field Strength
h	-	Convection Coefficient
H_i	-	Isoparametric Shape Functions
$\vec{J}$	-	Magnetic Current Density
[K]	-	Stiffness Matrix
$[K_t]$	-	Magnetic Permeability Matrix
[M]	-	"Consistent" Mass Matrix
n	-	Number of Nodes in an Element
$\{Q_B\}$	-	Element Heat Generation Vector
$\{Q_C\}$	-	Nodal Heat Flow Vector
$\{Q_S\}$	-	Boundary Heat Flow Vector
$\{q\}$	-	Element Heat Capacity Vector
STAEBL	-	Structural Tailoring of Engine Blades
TB	-	Boundary Temperature
W	-	Frequency

NOMENCLATURE (Concluded)

α	-	Surface Heat Transfer Coefficient
γ	-	Reciprocal Permeability
λ_i	-	ith Eigenvalue
μ	-	Magnetic Permeability
ρ	-	Resistivity
ϕ_i	-	ith Eigenvector

1.0 INTRODUCTION

This technical program is the work of the Engineering Mechanics and Life Management Section of the Aircraft Engine Business Group (AEBG) of the General Electric Company in response to NASA RFP 3-537260, "Coupled Structural/ Thermal/Electromagnetic (CSTEM) Analysis/Tailoring of Graded Composite Structures." The overall objective of this program is to develop and verify analysis and tailoring capability for graded composite engine structures taking into account the coupling constraints imposed by mechanical, thermal, acoustic, and electromagnetic loadings.

The first problem that will be attacked is the development of plate and shell finite elements capable of accurately simulating the structural/thermal/ electromagnetic response of graded composite engine structures. Because of the wide diversity of engine structures and the magnitudes of the imposed loadings, the analysis of these is very difficult and demanding when they are composed of isotropic, homogeneous materials. The added complexity of directional properties which can vary significantly through the thickness of the structure will challenge the state-of-the-art in finite element analysis. We are applying AEBG's 25 years of experience in developing and using structural analysis codes and the exceptional expertise of our University consultants toward the successful conclusion of this problem. To assist in this, we are drawing heavily on previously funded NASA programs.

We are drawing on NASA programs NAS3-23698, 3D Inelastic Analysis Methods For Hot Section Components, and NAS3-23687, Component Specific Modeling, in our development work on the plate and shell elements. In addition to these two programs, we will draw on NAS3-22767, Engine Structures Modeling Software System (ESMOSS), and NAS3-23272, Burner Liner Thermal/Structural Load Modeling, in Task III when we generate a total CSTEM Analysis System around these finite elements. This will guarantee that we are using the latest computer software technology and will produce an economical, flexible, easy to use system.

In our development of a CSTEM tailoring system, we will build on NASA Program NAS3-22525, Structural Tailoring of Engine Blades (STAEBL) and AEBG program, Automatic Improvement of Design (AID), in addition to the program system philosophy of ESMOSS. Because of the large number of significant parameters and design constraints, this tailoring system will be invaluable in promoting the use of graded composite structures.

All during this program, we will avail ourselves of the experience and advice of our Low Observables Technology group. This will be particularly true in the Task V proof-of-concept. Their input will be used to assure the relevancy of the total program.

Figure 1 shows our program and major contributions in flowchart form. This gives a visual presentation to the synergism that will exist between this program and other activities.

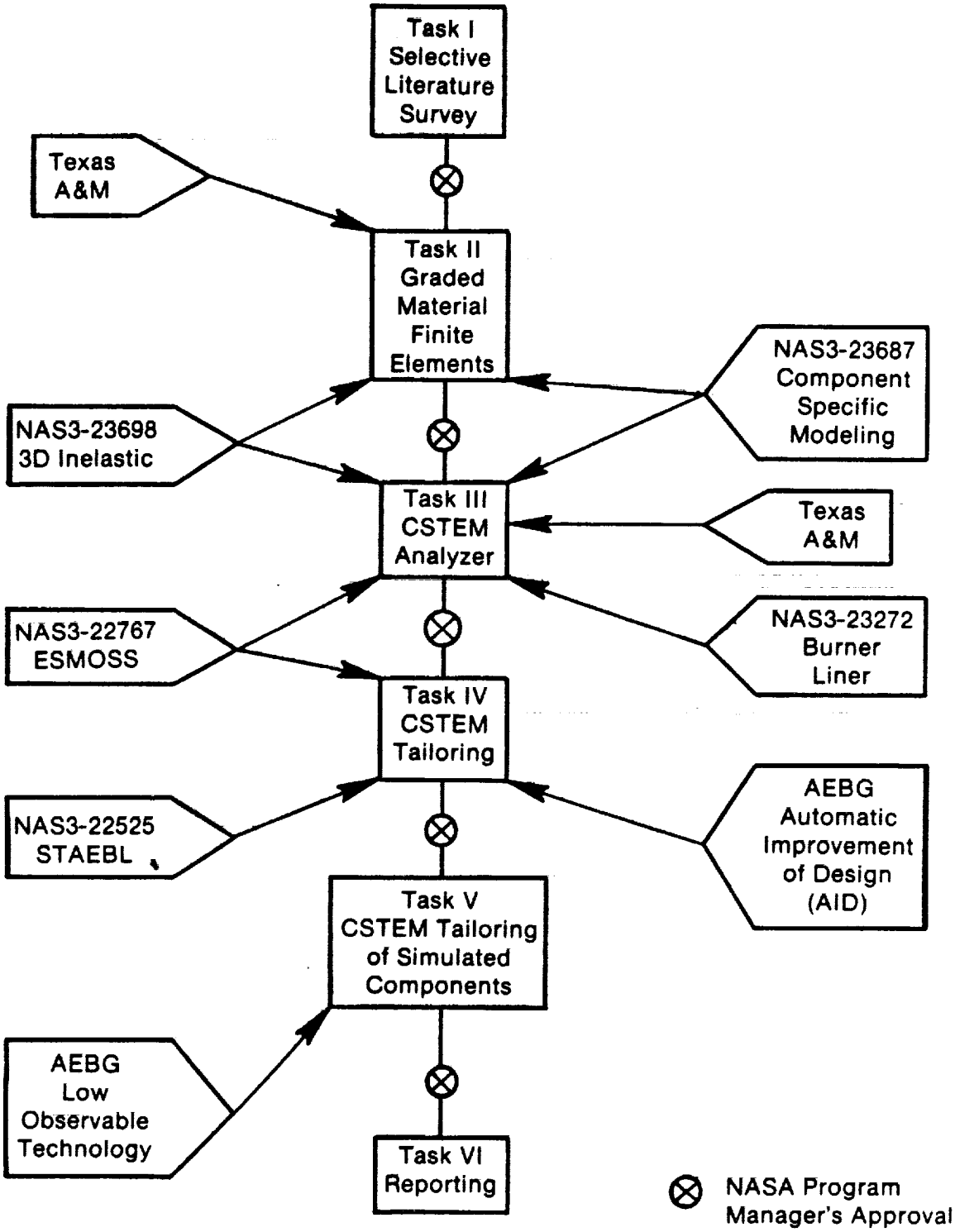

Figure 1. Program Flow Chart.

Figure 2 depicts an integrated analysis of composite structures currently under development in the composite users' community. The severe limitations of such a system are not highlighted because three major steps in the process are not shown. Figure 3 adds these steps. The analysis system really begins with a definition of geometry. A user then defines a finite element model simulating this geometry and the anticipated loading. The process then moves to defined Step 3. One cycle through the process ends with the prediction of individual ply average stresses and strains. Now comes a significant productivity drain, namely, manual intervention to evaluate these stresses and strains against strength and durability limits. Based on this, the user must decide to (1) change the finite element model, (2) change the composite laminate, (3) both of the above, or (4) stop here.

Obviously, there is a considerable cost savings to be obtained by selecting Number 4. The CSTEM system will obviate the reasons for selecting Number 4. This system, shown in Figure 4, begins with the definition of geometry, as before, but then proceeds to a definition of master regions which contain all of the necessary information about geometry, loading, and material properties. Step 3 is a constitutive model which develops the necessary structural, thermal, and electromagnetic properties based on a micromechanics approach. Furthermore, this constitutive model will contain the logic to generate the global finite element model based on the variation of the properties, as depicted in Figure 5. Using a nonlinear incremental technique, these global models will be solved for their structural, thermal, and electromagnetic response. Based on this response the global characteristics will be evaluated, with convergence criteria and decisions made on remodeling. Once the global characteristics meet the accuracy requirements, the local characteristics are interrogated and decisions made on remodeling because of strength, durability, or hereditary effects. Once this cycle has been stabilized, optimization will be performed based on design constraint. Our goal in Task II is to develop finite elements whose characteristics make this system possible. Although the structural properties have been highlighted, the thermal and electromagnetic properties have as much or more variation, and less work has been done in these areas.

1.1 EXECUTIVE SUMMARY

Meetings were held with designers and management of the Low Observables Sections to determine their requirements. It was learned that the generic problem was that structures designed for optimum electromagnetic capabilities often have nonoptimum thermal and structural capabilities. There is a need for a tool that can accurately and efficiently analyze and iterate among these three fields so that viable compromise designs can be generated. At present, no such tool exists.

Based on the Statement of Work and the results of the literature survey, we have established the 8-, 16-, and 20-noded isoparametric finite elements to be used to develop the CSTEM plate and shell element capabilities. These three elements meet the requirements for the plate elements. They have quadrilateral planform and are reducible to triangular planform, have nodes on the upper and lower surfaces, will meet accuracy requirements, and have

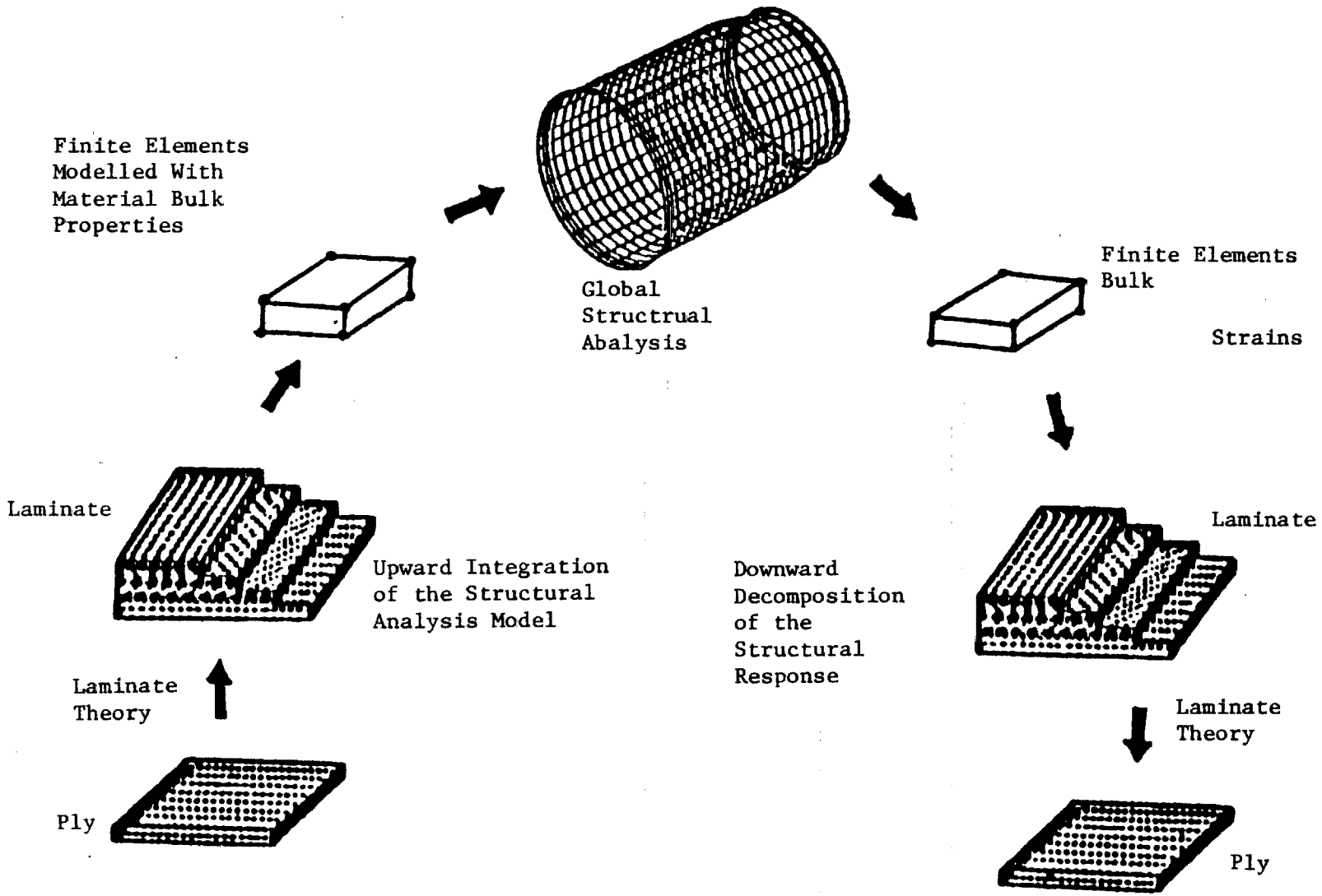

Figure 2. Composite Analysis System.

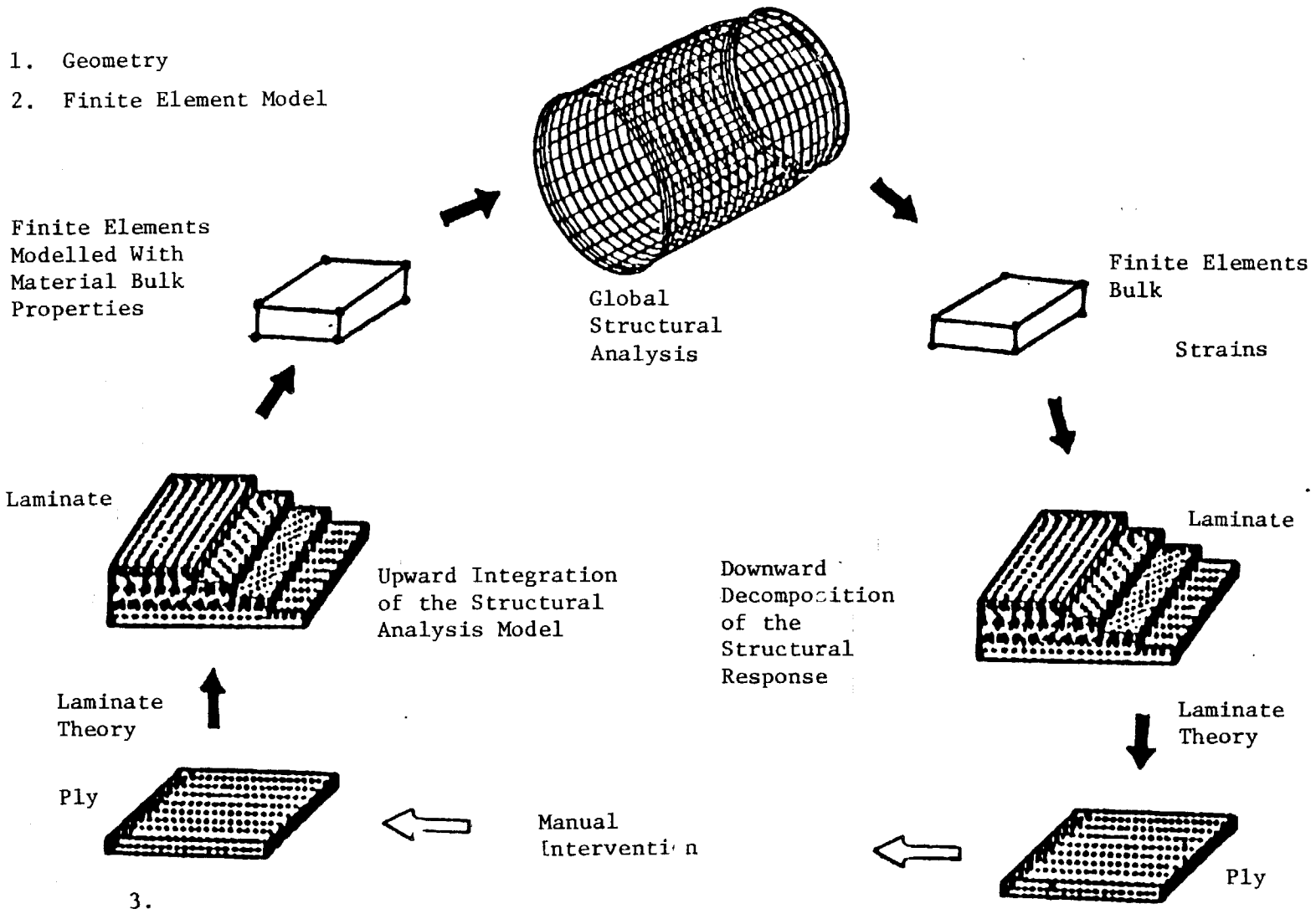

Figure 3. Total Composite Analysis System.

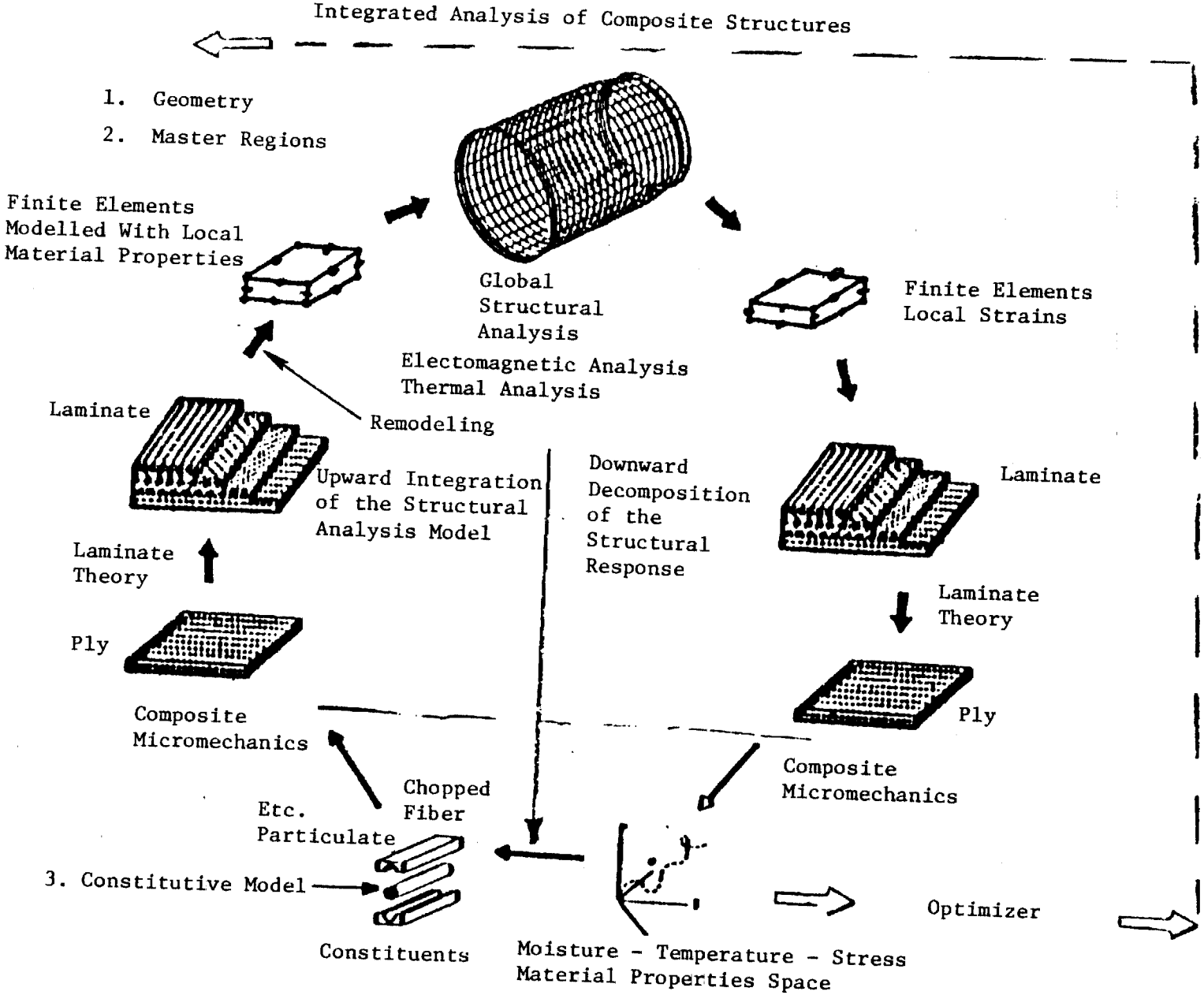

Figure 4. CSTEM System.

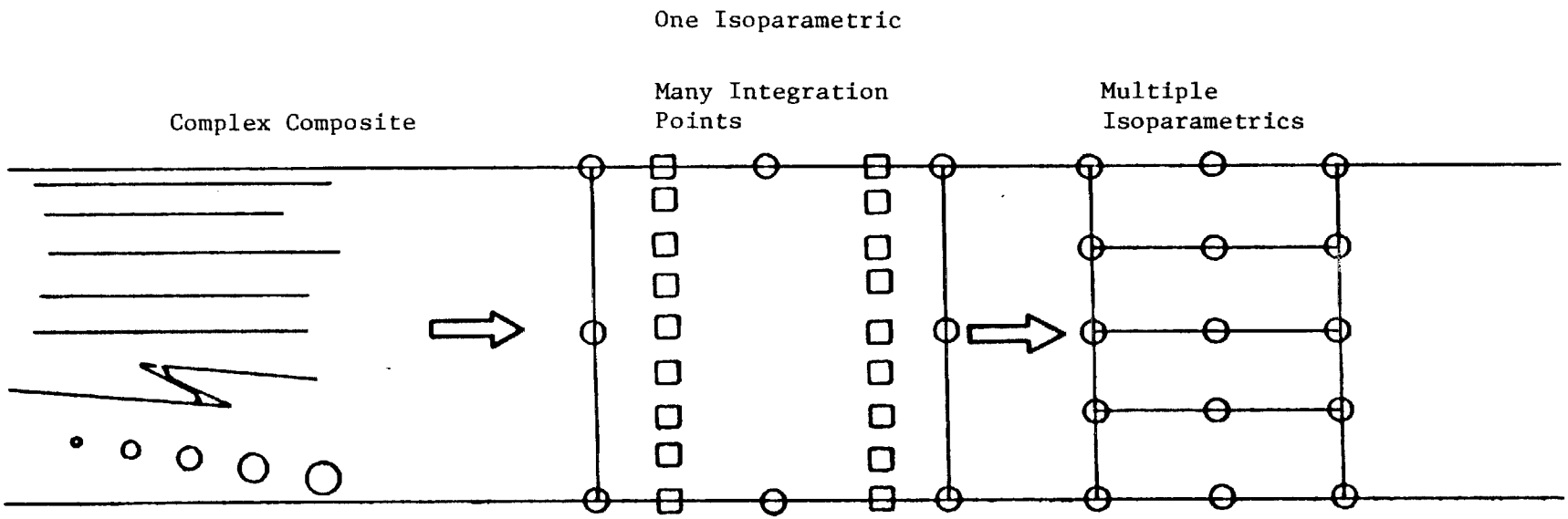

Figure 5. Constitutive Model - Structural Model Interaction.

the proper degrees of freedom to perform all three types of analyses. The 16- and 20-noded elements meet all of the requirements for the shell elements, including double curvature.

Having established the basic building block, progress has been made in the three major areas, that is, structural, thermal, and electromagnetic, while maintaining the maximum commonality in computer software, such as shape functions, Jacobians, et cetera.

Progress has occurred in the structural analysis area, as follows:

- Defined the nonlinear equilibrium system of equations, including large deformation effects. Established an incremental, updated Lagranian solution.
- Defined the overall programming architecture.
- Wrote the modular stiffness matrix subroutines.
- Wrote the modular mass matrix subroutines.
- Wrote the subroutines for modular load.
- Wrote subroutines for modular assembly and boundary conditions.
- Established the input data format and wrote input subroutines.
- Wrote the modular eigenvalue/eigenvector routines.
- Incorporated the linear constraint equations.
- Wrote a stress smoothing subroutine.
- Wrote a modular equation solver.
- Studied the micromechanics approach to stiffness formulation for composite elements.
- Ran the verification and validation cases for the elasticity and eigenanalysis capabilities.
- The file structure and data flow are currently under development.

In the thermal area, the following progress has been made:

- Anisotropic heat transfer equations have been defined for both linear and nonlinear conductivities and for steady-state and transient problems.
- All of the subroutines necessary to perform a linear, steady-state, anisotropic heat transfer problem have been written, making maximum use of the code that is common with the structural analysis.

In the electromagnetic area, the following progress has been made.

- Results of the literature survey have been studied.

- Dr. M.V.K. Chari, General Electric's expert on finite element electrical analysis, has been contacted.

- Finite element equations for the electromagnetic field problem have been established.

2.0 TECHNICAL PROGRESS

2.1 TASK I - SELECTIVE LITERATURE SURVEY

The first activity on this program was to perform a selective literature search using our internal General Electric data bases, the external COMPENDEX data base, and the literature supplied by the Texas A&M consultants. The pertinent articles turned up by this search are enumerated in Appendix A. Based on the results of this survey, it was proposed to the NASA Program Manager that the family of 8-, 16-, and 20-noded isoparametric elements be used for all three aspects of this program: structural, thermal, and electromagnetic.

The proposed plan of attack was:

- Work on three parallel efforts - structural, heat transfer, and electromagnetic
- Use an incremental updated Lagrangian approach for the large displacement structural problem.
- Handle the coupling among the fields by an iterative procedure.

2.2 TASK II - GRADED MATERIAL FINITE ELEMENTS

2.2.1 Task IIA - Plate Elements

The 8-, 16-, and 20-noded isoparametrics will be used as plate elements and shell elements. As plate elements, there will be a restriction that the midsurfaces be in a plane. This restriction will be the only difference between the plate and shell elements and, primarily, affects the program input. A simpler geometric and loading input can be used. Beyond this, all of the technical requirements are the same as for the shell elements. These will be discussed in the next section.

2.2.2 Task IIB - Shell Elements

AEBG has developed and used many different plate and shell elements. The elements to be used in this program are the 8-, 16-, and 20-noded isoparametric elements. These have been used both as plates and as doubly curved shells for both linear and nonlinear material behavior. A review of these elements follows.

Isoparametric Solid Elements

The isoparametric solid elements permit the modeling of any general three-dimensional (3D) object, since the elements represent a discretization

of the object into finite elements which are 3D continuous representations. The basic term "isoparametric" means that the elements utilize the same interpolating functions (also called "shape functions") to interpolate geometry, displacements, strains, and temperatures. It is, therefore, important that the user be aware that not just any displacement, geometry, and temperature field to be analyzed is necessarily compatible with a given element mesh. This is particularly true where high temperature or strain gradients occur. The following sections discuss the basic element formulation assumptions.

Shape functions are used to describe the variation of some function G within an element in terms of the nodal point values.

$$G(x,y,z) = \sum_{i=1}^{n} H_i G_i(x_i,y_i,z_i)$$

where

$G(x,y,z)$ = the value of the function (such as displacement, temperature) at any point with coordinates (x,y,z) within an element

$G(x_i,y_i,z_i)$ = the value of the function at node point i

H_i = the element "shape function" associated with node i

n = the number of nodes describing intraelement variation.

In order to ensure monotonic convergence to the correct results, shape functions must satisfy several requirements. Satisfaction of these requirements results in convergence from an upper bound. These displacement function requirements are:

- They must include all possible rigid body displacements
- They must be able to represent constant strain states
- They must be differentiable within elements and compatible between adjacent elements.

While the above conditions prove valuable for establishing upper bounds for solutions, they are not essential. Incompatible displacement modes are widely and successfully used. Their principal disadvantage is that stiffness may no longer be bounded from above.

Curvilinear coordinates are introduced into the isoparametric concept to overcome the difficulty of formulating shape functions in global Cartesian coordinates. Also, generality in element geometry definition is obtained by this process.

A local curvilinear coordinate system (r,s,t), which ranges from -1 to 1 within each element, is introduced in which shape functions are formulated. Also, a mapping from curvilinear to global coordinates is defined. A typical two dimensional element is shown in Figure 6.

The same polynomial terms used in the Cartesian coordinates are used but with the curvilinear coordinates r,s,t replacing x, y, and z to generate shape functions. The r, s, and t coordinates are the same for all global element configurations.

Typical finite element equilibrium equations:

1. Structural

$$[M]\{\ddot{u}_i\} + [C]\{\dot{u}_i\} + [K]\{u_i\} = \{F_B\} + \{F_S\} + \{F_I\} + \{F_C\} + \{F_{NL}\}$$

$[M] = \int_V \rho [H]^T [H] dv$ "Consistent" mass matrix

$[C]$ = Damping matrix

$[K] = \int_V [B]^T [D] [B] dv$ Stiffness matrix

$\{F_B\} = \int_V [H]^T \{f_B\} dv$ Body forces

$\{F_S\} = \int_S [H^S]^T \{f_S\} dS$ Surface tractions

$\{F_I\} = \int_V [B]^T [D] \{\varepsilon_T\} dv$ Initial strains

$\{F_{NL}\} = \int_V [B]^T [D] \{\varepsilon_{NL}\} dv$ Nonlinear strains

where

$\{ui\}T = [u_1\ v_1\ w_1\ u_2\ v_2\ w_2 \ldots .]$

$\{u\}T = [u\ v\ w]$

$\{u\} = [H]\{u_i\}$

$\{\varepsilon\} = [B]\{u_i\}$

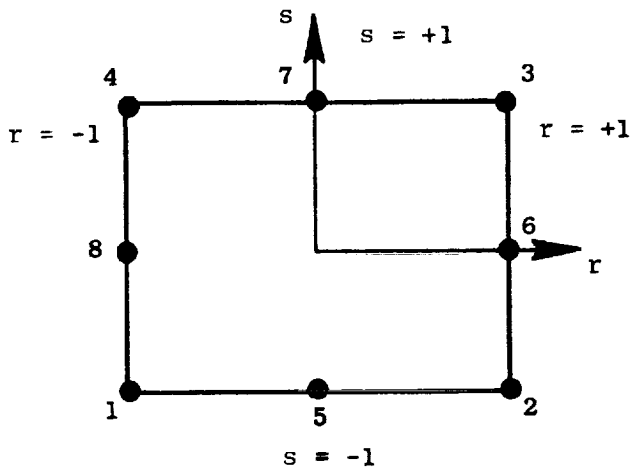

(a) Curvilinear Coordinates

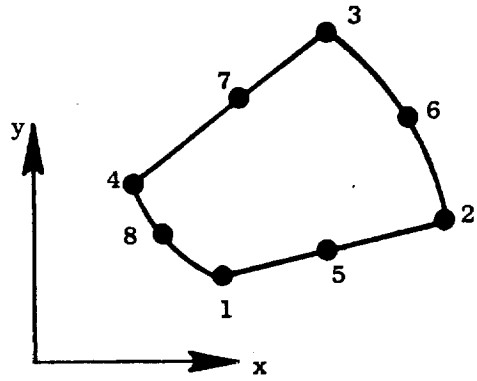

(b) Global Coordinates

Figure 6. Typical Two-Dimensional Element.

$$\{\sigma\} = [D]\{\epsilon^e\} = [D](\{\epsilon^{TOT}\}-\{\epsilon^{THERM}\}-\{\epsilon_{NL}\})$$

$$\{f_B\}^T = [f_{Bx}\ f_{By}\ f_{Bz}]$$

$$\{f_S\}^T = [f_{Sx}\ f_{Sy}\ f_{Sz}]$$

2. Thermal

$$[q]\{\dot{T}_i\} + [K]\{T_i\} = \{Q_B\} + \{Q_S\} + \{Q_C\}$$

$[q] = \int_V c[H]^T[H]dv$ Element heat capacity

$[K] = \int_V [B]^T[R][B]dv + \int_{S_2} \alpha\ [H^S]^T[H^s]dS_2$ Element conductivity

$[Q_B] = \int_V [H]^T\{q_B\}dv$ Element heat generation

$[Q_S] = \int_{S_1} [H^{S1}]^T\{q_S\}dS_1 + \int_S \alpha[H^S]^T T_B dS_2$ Boundary heat flow

$\{Q_C\}$ = Concentrated heat flow

where

$\{T_i\}^T = [T_1\ T_2\ T_3 \ldots]$

$\{T\} = [H]\{T_i\}$

$\{q\} = [B]\{T_i\}$

C = Specific heat

T_B = Boundary temperature

α = Surface heat transfer coefficient

3. Electromagnetic

$$\gamma[S]\{A_i\} + \gamma[D]\{A_i\} + \gamma[E]\{A_i\} + \frac{Jw}{\rho}[T]\{A_i\} = [T]\{J_i\}$$

where [S], [D], [E], and [T] are functions of [H].

$\{A_i\}$ = Nodal point values of potential

$\{J_i\}$ = Nodal point values of forcing functions

γ = Reciprocal permeability

w = Frequency

ρ = Resistivity

Other field problems have similar finite element expressions.

8-Noded Solid

The 8-noded solid element utilizes a formal mapping technique with displacement functions defined by a series of interpolating polynomials called "shape functions." In this manner, an arbitrary solid of six faces can be mapped from a parent coordinate system as shown in Figure 7. The numbering sequence must be as shown in this figure, except the user may define the nodes N1 and N5 as any convenient nodes on the solid. Note that node N1 has the parent coordinates (r,s,t) = (1,1,1). Once this has been established by the user, all face definition given later in this section is established.

The shape functions for this element are as follows:

$$H_1 = (1 + r)(1 + s)(1 + t)/8$$

$$H_2 = (1 - r)(1 + s)(1 + t)/8$$

$$H_3 = (1 - r)(1 - s)(1 + t)/8$$

$$H_4 = (1 + r)(1 - s)(1 + t)/8$$

$$H_5 = (1 + r)(1 + s)(1 - t)/8$$

$$H_6 = (1 - r)(1 + s)(1 - t)/8$$

$$H_7 = (1 - r)(1 - s)(1 - t)/8$$

$$H_8 = (1 + r)(1 - s)(1 - t)/8$$

Since this element has linear displacements on an edge, the ability to model the deformation due to bending is not possible, and the element will be overly stiff in bending. To overcome this, the addition of non-nodal degrees of freedom can be used as an option. These are called "incompatible modes," and are condensed out of the element stiffness after stiffness generation, leaving 24 degrees of freedom per element. The interpolation for all element properties and displacements is given by:

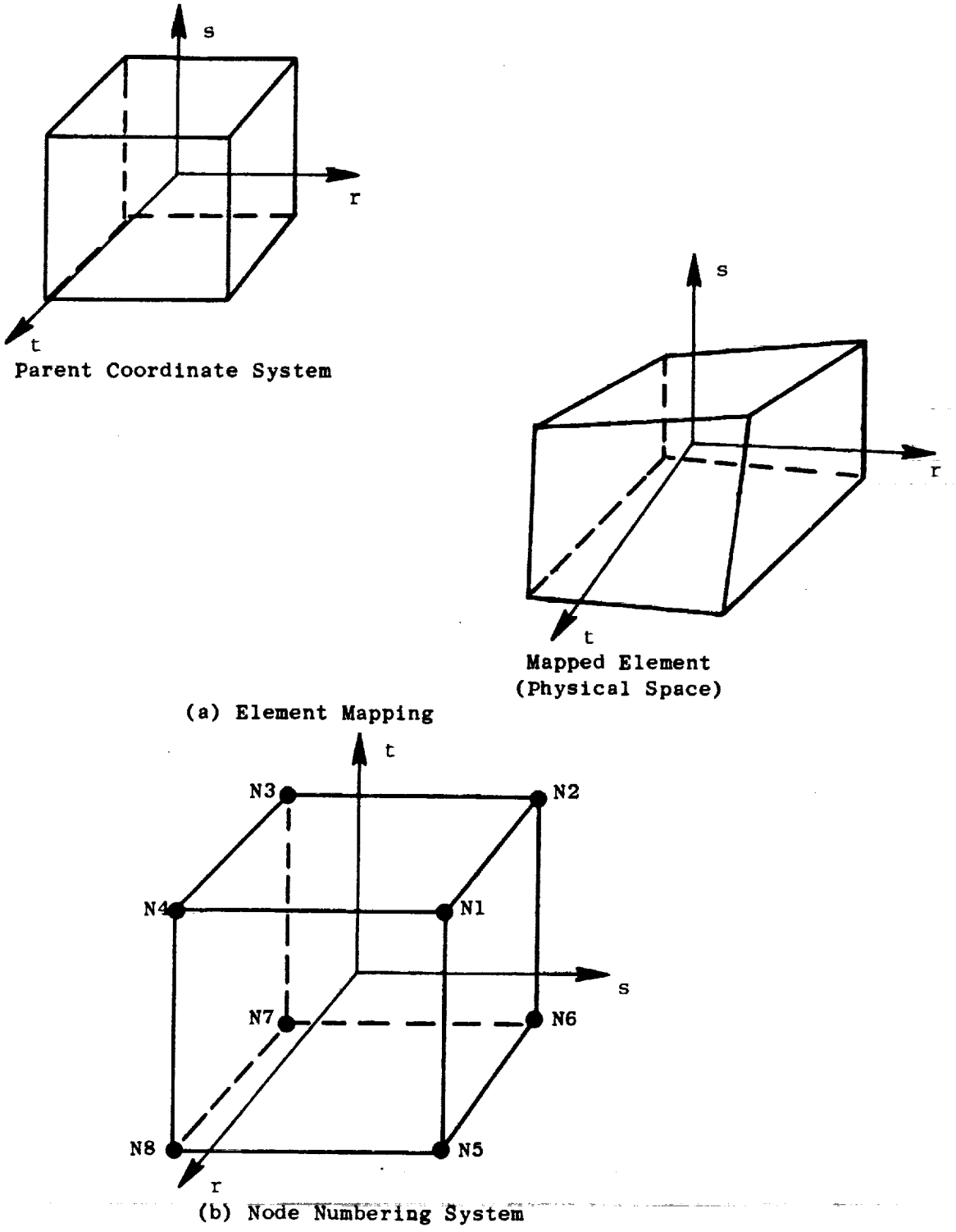

Figure 7. Eight-Noded Solid Coordinate and Node Numbering System.

$$u = \sum_{i=1}^{8} H_i U_i + \left(1 - r^2\right) a_1 + \left(1 - s^2\right) a_2 + \left(1 - t^2\right) a_3$$

$$v = \sum_{i=1}^{8} H_i V_i + \left(1 - r^2\right) a_4 + \left(1 - s^2\right) a_5 + \left(1 - t^2\right) a_6$$

$$w = \sum_{i=1}^{8} H_i W_i + \left(1 - r^2\right) a_7 + \left(1 - s^2\right) a_8 + \left(1 - t^2\right) a_9$$

where a_1 through a_9 are the extra "generalized" degrees of freedom which are condensed out. The user is given the option to include or not include the incompatible modes. In general, they should be included only when bending across an element is expected to be significant and only for elastic analyses.

Given the coordinate system (r,s,t) as previously established, we can also now define the face numbering conventions and order of nodes on a face. These definitions are needed to establish conventions for inputting pressure loads on the element and number of faces when displaying surface stresses on the faces. These conventions are summarized below:

Face No.	Location	Nodes and Node Order on Face			
1	r = +1	N1	N4	N8	N5
2	s = +1	N1	N5	N6	N2
3	t = +1	N1	N2	N3	N4
4	r = -1	N7	N3	N2	N6
5	s = -1	N7	N8	N4	N3
6	t = -1	N7	N6	N5	N8

This element has been formulated with variable temperature and general orthotropic material properties. During numerical integration for stiffness and equivalent nodal forces due to thermals, plasticity, and creep, the material properties at each integration point are evaluated at the temperature of that integration point. A Gauss integration scheme is used, and the user may choose an integration order of 2, 3, or 4 points in each direction (r,s,t).

16-Noded Solid

The 16-noded solid follows the same type of development for stiffness and loads as the 8-noded solid and, like the 8-noded solid, it has three displacement degrees of freedom per node, thus a total of 48 degrees of freedom on the element. Since this element has higher order interpolating functions in two directions on an edge, this element is sometimes called a "thick shell" element, as it can be used with reasonable approximation in this type of analysis where the shell thickness is in the t direction.

The node numbering sequence must be as shown in Figure 8, except that the user can define the location of Nodes N_1 and N_9 as desired. Note that Node N_1 has the parent coordinates $(r,s,t) \equiv (1,1,1)$. Since this has been established, all face numbering is then defined.

Starting with the basic interpolating functions for the corners, we define:

$G1 = (1 + r)\ (1 + s)\ (1 + t)/8$ $\qquad$ $G9 = (1 + r)\ (1 + s)\ (1 - t)/8$

$G3 = (1 - r)\ (1 + s)\ (1 + t)/8$ $\qquad$ $G11 = (1 - r)\ (1 + s)\ (1 - t)/8$

$G5 = (1 - r)\ (1 - s)\ (1 + t)/8$ $\qquad$ $G13 = (1 - r)\ (1 - s)\ (1 - t)/8$

$G7 = (1 + r)\ (1 - s)\ (1 + t)/8$ $\qquad$ $G15 = (1 + r)\ (1 - s)\ (1 - t)/8$

Then, for the midside nodes, the shape functions are:

$$H_2 = (1 - r)\ (1 + s)\ (1 + t)/4$$

$$H_4 = (1 - r)\ (1 - s)\ (1 + t)/4$$

$$H_6 = (1 - r)\ (1 - s)\ (1 + t)/4$$

$$H_8 = (1 + r)\ (1 - s)\ (1 + t)/4$$

$$H_{10} = (1 - r)\ (1 + s)\ (1 - t)/4$$

$$H_{12} = (1 - r)\ (1 - s)\ (1 - t)/4$$

$$H_{14} = (1 - r)\ (1 - s)\ (1 - t)/4$$

$$H_{16} = (1 + r)\ (1 - s)\ (1 - t)/4$$

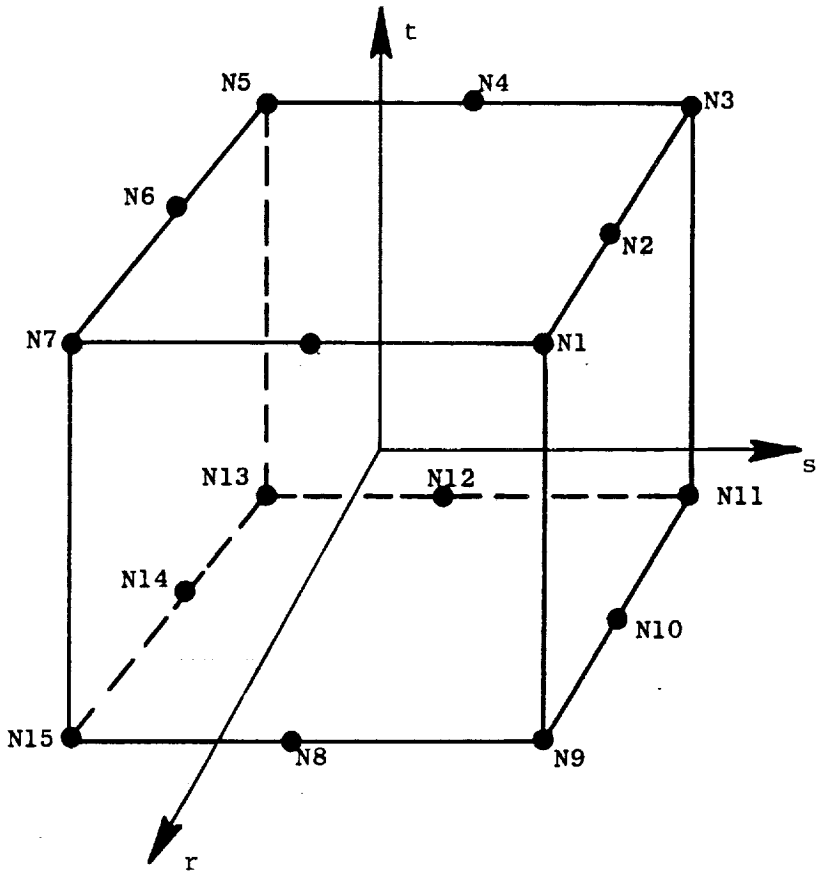

Figure 8. Sixteen-Noded Solid Coordinate and Node Numbering System.

and for the corner nodes, the modified shape functions are:

$$H_1 = G_1 - (H_2 + H_8)/2$$

$$H_3 = G_3 - (H_2 + H_4)/2$$

$$H_5 = G_5 - (H_4 + H_6)/2$$

$$H_7 = G_7 - (H_6 + H_8)/2$$

$$H_9 = G_9 - (H_{10} + H_{16})/2$$

$$H_{11} = G_{11} - (H_{10} + H_{12})/2$$

$$H_{13} = G_{13} - (H_{12} + H_{14})/2$$

$$H_{15} = G_{15} - (H_{14} + H_{16})/2$$

As in the case of the 8-noded solid, the user may use an option to specify that certain extra generalized degrees of freedom be added to introduce "incompatible modes" for bending. If through-thickness bending in the t direction is significant, these modes will prevent the element from being overly stiff. These generalized degrees of freedom are condensed out after stiffness formulation, leaving only the 48 nodal degrees of freedom. The complete element interpolating functions, used to interpolate displacements, etc., are thus:

$$u = \sum_{i=1}^{16} H_i U_i + \sum_{i=1}^{6} \bar{H}_i a_i$$

$$v = \sum_{i=1}^{16} H_i V_i + \sum_{i=1}^{6} \bar{H}_i b_i$$

$$w = \sum_{i=1}^{16} H_i W_i + \sum_{i=1}^{6} \bar{H}_i c_i$$

where the interpolating function coefficients for the generalized displacements are:

$$\bar{H}_1 = r\,(1 - r^2)\quad \bar{H}_2 = s\,(1 - s^2)\quad \bar{H}_3 = (1 - t^2)$$

$$\bar{H}_4 = rs\,(1 - r^2)\quad \bar{H}_5 = rs\,(1 - s^2)\quad \bar{H}_6 = (1 - r^2)\,(1 - s^2)$$

and the variables a_1 to a_6, b_1 to b_6, and c_1 to c_6 are the 18 generalized displacements which are condensed out after stiffness formulation.

Given the coordinate system (r,s,t) as previously established, we can also now define the face numbering conventions and order of nodes on a face. These definitions are needed to establish conventions for inputting pressure levels on the element and numbering of faces when displaying surface stresses on the faces. These conventions are summarized below:

Face No.	Location	Nodes and Node Order on Face							
1	r = +1	N1	N8	N7	N15	N16	N9		
2	s = +1	N1	N9	N10	N11	N3	N2		
3	t = +1	N13	N2	N3	N4	N5	N6	N7	N8
4	r = -1	N13	N4	N4	N3	N11	N12		
5	s = -1	N13	N14	N15	N7	N6	N5		
6	t = -1	N13	N12	N11	N10	N9	N16	N15	N14

This element has been formulated with variable temperature general orthotropic material properties. During numerical integration for stiffness and equivalent nodal forces due to thermals, plasticity, and creep, the material properties at each integration point are evaluated at the temperature of that integration point. A Gauss integration scheme is used, and the user may choose an integration order of 2, 3, or 4 points in each direction (r,s,t).

Twenty-Noded Isoparametric Finite Element

Figure 9 shows the representation and mapping of the 20-noded isoparametric finite element in the the global (physical space) x, y, z coordinate system and the parent (barycentric) r, s, t, coordinate system. The transformation maps any global element into the same parent element with coordinate ranges of

$$-1 \leq r \leq +1$$

$$-1 \leq S \leq +1$$

$$-1 \leq t \leq +1$$

Figure 10 shows the node numbering in the parent coordinate system. Table 1 gives the coordinate of each node.

Let

(u, v, w) = Displacements of a point in the (x, y, z) directions

(u_i, v_i, w_i), $i = 1, 20$ = Displacements of the nodes in the (x, y, z) directions

$\{d\} = [u, v, w]^T$

$\{d_i\} = [u_i, v_i, w_i]^T$

Then for any point within the domain of the element:

$$u = \sum_{i=1}^{20} H_i u_i = H_i u_i$$

$$v = \sum_{i=1}^{20} H_i v_i = H_i v_i$$

$$w = \sum_{i=1}^{20} H_i w_i = H_i w_i$$

$$\begin{bmatrix} u \\ v \\ w \end{bmatrix} = \begin{bmatrix} H_i & 0 & 0 \\ 0 & H_i & 0 \\ 0 & 0 & H_i \end{bmatrix} \begin{bmatrix} u_i \\ v_i \\ w_i \end{bmatrix}$$

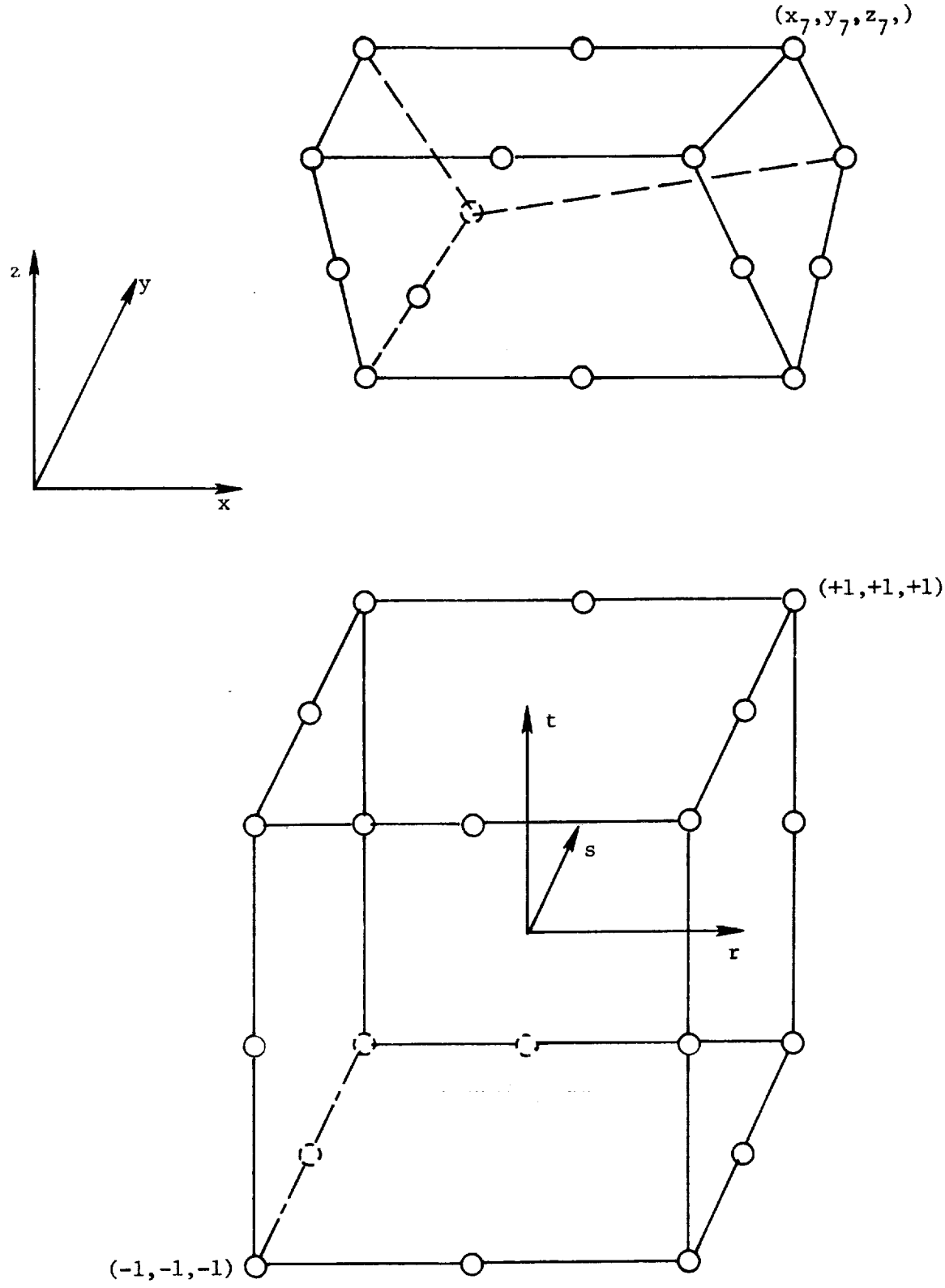

Figure 9. Twenty-Noded Isoparametric Finite Element Mapping.

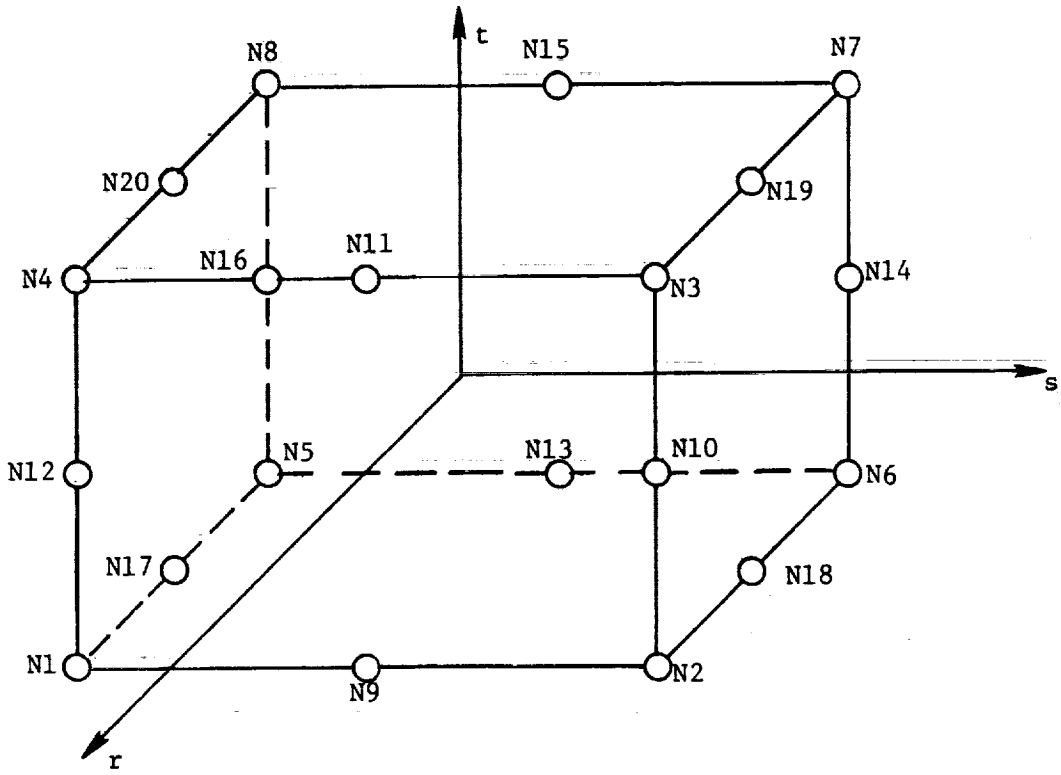

Figure 10. Twenty-Noded Isoparametric Finite Element Element Mapping.

Table 1. Nodal Coordinates for 20-Nodal Element.

Node Number	r	s	t
1	1	-1	-1
2	1	1	-1
3	1	1	1
4	1	-1	1
5	-1	-1	-1
6	-1	1	-1
7	-1	1	1
8	-1	-1	1
9	1	0	-1
10	1	1	0
11	1	0	1
12	1	-1	0
13	-1	0	-1
14	-1	1	0
15	-1	0	1
16	-1	-1	0
17	0	-1	-1
18	0	1	-1
19	0	1	1
20	0	-1	1

where the H_i in terms of the parent coordinate system are given as follows. The basic corner noded shape functions are

$$G_1 = (1+r)(1-s)(1-t)/8$$

$$G_2 = (1+r)(1+s)(1-t)/8$$

$$G_3 = (1+r)(1+s)(1+t)/8$$

$$G_4 = (1+r)(1-s)(1+t)/8$$

$$G_5 = (1-r)(1-s)(1-t)/8$$

$$G_6 = (1-r)(1+s)(1-t)/8$$

$$G_7 = (1-r)(1+s)(1+t)/8$$

$$G_8 = (1-r)(1-s)(1+t)/8$$

The midside node shape functions are

$$H_9 = (1+r)(1-s^2)(1-t)/4$$

$$H_{10} = (1+r)(1+s)(1-t^2)/4$$

$$H_{11} = (1+r)(1-s^2)(1+t)/4$$

$$H_{12} = (1+r)(1-s)(1-t^2)/4$$

$$H_{13} = (1-r)(1-s^2)(1-t)/4$$

$$H_{14} = (1-r)(1+s)(1-t^2)/4$$

$$H_{15} = (1-r)(1-s^2)(1+t)/4$$

$$H_{16} = (1-r)(1-s)(1-t^2)/4$$

$$H_{17} = (1-r^2)(1-s)(1-t)/4$$

$$H_{18} = (1-r^2)(1+s)(1-t)/4$$

$$H_{19} = (1-r^2)(1+s)(1+t)/4$$

$$H_{20} = (1-r^2)(1-s)(1+t)/4$$

The modified corner node shape functions are

$$H_1 = G_1 - (H_9+H_{12}+H_{17})/2$$

$$H_2 = G_2 - (H_9+H_{10}+H_{18})/2$$

$$H_3 = G_3 - (H_{10}+H_{11}+H_{19})/2$$

$$H_4 = G_4 - (H_{11}+H_{12}+H_{20})/2$$

$$H_5 = G_5 - (H_{13}+H_{16}+H_{17})/2$$

$$H_6 = G_6 - (H_{13}+H_{14}+H_{18})/2$$

$$H_7 = G_7 - (H_{14}+H_{15}+H_{19})/2$$

$$H_8 = G_8 - (H_{15}+H_{16}+H_{20})/2$$

In a three-dimensional context, the relations between the displacements and the strains are given by the following.

Six Strain-Displacement Relations

$$\varepsilon_{xx} = \frac{\partial u}{\partial x}$$

$$\varepsilon_{yy} = \frac{\partial v}{\partial y}$$

$$\varepsilon_{zz} = \frac{\partial w}{\partial z}$$

$$\varepsilon_{xy} = \frac{1}{2}\gamma_{xy} = \frac{1}{2}\left(\frac{\partial u}{\partial y} + \frac{\partial v}{\partial x}\right)$$

$$\varepsilon_{yz} = \frac{1}{2}\gamma_{yz} = \frac{1}{2}\left(\frac{\partial v}{\partial z} + \frac{\partial w}{\partial y}\right)$$

$$\varepsilon_{zx} = \frac{1}{2}\gamma_{zx} = \frac{1}{2}\left(\frac{\partial w}{\partial x} + \frac{\partial u}{\partial z}\right)$$

Therefore, the strain at any point within the elements domain is given by the following.

$$\begin{bmatrix} \varepsilon_x \\ \varepsilon_y \\ \varepsilon_z \\ \gamma_{xy} \\ \gamma_{yz} \\ \gamma_{zx} \end{bmatrix} = \begin{bmatrix} \frac{\partial u}{\partial x} \\ \frac{\partial v}{\partial y} \\ \frac{\partial w}{\partial z} \\ \frac{\partial u}{\partial y} + \frac{\partial v}{\partial x} \\ \frac{\partial v}{\partial z} + \frac{\partial w}{\partial y} \\ \frac{\partial w}{\partial x} + \frac{\partial u}{\partial z} \end{bmatrix} = \begin{bmatrix} \frac{\partial H_i}{\partial x} & 0 & 0 \\ 0 & \frac{\partial H_i}{\partial y} & 0 \\ 0 & 0 & \frac{\partial H_i}{\partial z} \\ \frac{\partial H_i}{\partial y} & \frac{\partial H_i}{\partial x} & 0 \\ 0 & \frac{\partial H_i}{\partial z} & \frac{\partial H_i}{\partial y} \\ \frac{\partial H_i}{\partial z} & 0 & \frac{\partial H_i}{\partial x} \end{bmatrix} \begin{bmatrix} u_i \\ v_i \\ w_i \end{bmatrix}$$

or

$$\{\varepsilon\} = [B_i] \{d_i\}$$

$$\varepsilon = B_i \, d_i$$

Since the Hi are defined in the parent coordinate system, we need to define the derivatives with respect to the global coordinate system by the chain rule of differentiation.

$$\frac{\partial H_i}{\partial x} = \frac{\partial H_i}{\partial r}\frac{\partial r}{\partial x} + \frac{\partial H_i}{\partial s}\frac{\partial s}{\partial x} + \frac{\partial H_i}{\partial t}\frac{\partial t}{\partial x}$$

$$\frac{\partial H_i}{\partial y} = \frac{\partial H_i}{\partial r}\frac{\partial r}{\partial y} + \frac{\partial H_i}{\partial s}\frac{\partial s}{\partial y} + \frac{\partial H_i}{\partial t}\frac{\partial t}{\partial y}$$

$$\frac{\partial H_i}{\partial z} = \frac{\partial H_i}{\partial r}\frac{\partial r}{\partial z} + \frac{\partial H_i}{\partial s}\frac{\partial s}{\partial z} + \frac{\partial H_i}{\partial t}\frac{\partial t}{\partial z}$$

To produce the required terms for the above expressions we need to develop the Jacobian matrix.

$$J = \begin{bmatrix} \frac{\partial x}{\partial r} & \frac{\partial y}{\partial r} & \frac{\partial z}{\partial r} \\ \frac{\partial x}{\partial s} & \frac{\partial y}{\partial s} & \frac{\partial z}{\partial s} \\ \frac{\partial x}{\partial t} & \frac{\partial y}{\partial t} & \frac{\partial z}{\partial t} \end{bmatrix}$$

$$J = \begin{bmatrix} \frac{\partial H_i}{\partial r} x_i & \frac{\partial H_i}{\partial r} y_i & \frac{\partial H_i}{\partial r} z_i \\ \frac{\partial H_i}{\partial s} x_i & \frac{\partial H_i}{\partial s} y_i & \frac{\partial H_i}{\partial s} z_i \\ \frac{\partial H_i}{\partial t} x_i & \frac{\partial H_i}{\partial t} y_i & \frac{\partial H_i}{\partial t} z_i \end{bmatrix}$$

$$J = \begin{bmatrix} \frac{\partial H_1}{\partial r} & \frac{\partial H_2}{\partial r} & \cdots & \frac{\partial H_{20}}{\partial r} \\ \frac{\partial H_1}{\partial S} & \frac{\partial H_2}{\partial S} & \cdots & \frac{\partial H_{20}}{\partial S} \\ \frac{\partial H_1}{\partial t} & \frac{\partial H_2}{\partial t} & \cdots & \frac{\partial H_{20}}{\partial t} \end{bmatrix} \begin{bmatrix} x_1 & y_1 & z_1 \\ x_2 & y_2 & z_2 \\ \cdot & \cdot & \cdot \\ \cdot & \cdot & \cdot \\ \cdot & \cdot & \cdot \\ \cdot & \cdot & \cdot \\ \cdot & \cdot & \cdot \\ \cdot & \cdot & \cdot \\ x_{20} & y_{20} & z_{20} \end{bmatrix}$$

Inverting this Jacobian gives the following:

$$J^{-1} = \begin{bmatrix} \frac{\partial r}{\partial x} & \frac{\partial s}{\partial x} & \frac{\partial t}{\partial x} \\ \frac{\partial r}{\partial y} & \frac{\partial s}{\partial y} & \frac{\partial t}{\partial y} \\ \frac{\partial r}{\partial z} & \frac{\partial s}{\partial z} & \frac{\partial t}{\partial z} \end{bmatrix}$$

This is equivalent to the following:

$$J^{-1} = \frac{1}{\det J} \begin{bmatrix} \frac{\partial z}{\partial t} & -\frac{\partial z}{\partial s} & -\frac{\partial z}{\partial r} \\ -\frac{\partial y}{\partial t} & \frac{\partial y}{\partial s} & -\frac{\partial y}{\partial r} \\ -\frac{\partial x}{\partial t} & -\frac{\partial x}{\partial s} & \frac{\partial x}{\partial r} \end{bmatrix}$$

This gives all the necessary terms for the B matrix and therefore the ability to compute strain at any point within the element domain.

$$\varepsilon(x,y,z) = B(x,y,z)_i \; d_i$$

$$\varepsilon = \begin{bmatrix} \frac{\partial H_1}{\partial x} & 0 & 0 & \frac{\partial H_2}{\partial x} & 0 & 0 & \cdots & \frac{\partial H_{20}}{2x} & 0 & 0 \\ 0 & \frac{\partial H_i}{\partial y} & 0 & 0 & \frac{\partial H_2}{\partial y} & 0 & \cdots & 0 & \frac{\partial H_{20}}{\partial y} & 0 \\ 0 & 0 & \frac{\partial H_i}{\partial z} & 0 & 0 & \frac{\partial H_i}{\partial z} & \cdots & 0 & 0 & \frac{\partial H_{20}}{\partial z} \end{bmatrix} \begin{bmatrix} x_1 \\ y_1 \\ z_1 \\ x_2 \\ y_2 \\ z_2 \\ . \\ . \\ . \\ x_{20} \\ y_{20} \\ z_{20} \end{bmatrix}$$

The volume of the element is given by the following integral:

$$V = \int_{-1}^{+1} \int_{-1}^{+1} \int_{-1}^{+1} \text{detJ } drdsdt$$

The various structural, thermal, and electromagnetic quantities will be determined by integrals over the volume, which takes the following form.

$$F_{ij} = \int_{-1}^{+1} \int_{-1}^{+1} \int_{-1}^{+1} g_{ij} \text{ detJ } drdsdt$$

Or, letting $G_{ij} = g_{ij}$ detJ

$$F_{ij} = \int_{-1}^{+1} \int_{-1}^{+1} \int_{-1}^{+1} G_{ij} \, drdsdt$$

This is normally evaluated by numerical integration of some form.

$$F_{ij} = \sum_{a=1}^{m} \sum_{b=1}^{n} \sum_{c=1}^{o} G(r_a, s_b, t_c) \, W_a \, W_b \, W_c$$

where m x n x o sampling points are used and W_a, W_b, W_c are the weighting factors for location r_a, s_b, t_c. One of our major efforts is the investigation of various numerical integration techniques with respect to the requirements of CSTEM. Table 2 gives the locations and weights for up to the fourth order Glauss-Legendre Quadrature. Table 3 gives the information for up to sixth order Newton-Cotes (even interval) quadrature.

Table 2. Gauss-Legendre Quadrature.

Integration Order	i	r_i	w_i
2	I	$+1/\sqrt{3}$	+1
	II	$-1/\sqrt{3}$	+1
3	I	0	8/9
	II	$+\sqrt{0.6}$	5/9
	III	$-\sqrt{0.6}$	5/9
4	I	$\sqrt{\frac{3+\sqrt{4.8}}{7}}$	$\frac{1}{2}-\frac{\sqrt{30}}{36}$
	II	$-\sqrt{\frac{3+\sqrt{4.8}}{7}}$	$\frac{1}{2}-\frac{\sqrt{30}}{36}$
	III	$\sqrt{\frac{3-\sqrt{4.8}}{7}}$	$\frac{1}{2}+\frac{\sqrt{30}}{36}$
	IV	$-\sqrt{\frac{3-\sqrt{4.8}}{7}}$	$\frac{1}{2}+\frac{\sqrt{30}}{36}$

Table 3. Newton-Cotes Quadrature.

$$\int_0^b F(r)dr = (b-a)\sum_{i=0}^{n} C_i^n F_i + R_n$$

No. of Intervals n	C_0^n	C_1^n	C_2^n	C_3^n	C_4^n	C_5^n	C_6^n
1	$\frac{1}{2}$	$\frac{1}{2}$					
2	$\frac{1}{6}$	$\frac{4}{6}$	$\frac{1}{6}$				
3	$\frac{1}{8}$	$\frac{3}{8}$	$\frac{3}{8}$	$\frac{1}{8}$			
4	$\frac{7}{90}$	$\frac{32}{90}$	$\frac{12}{90}$	$\frac{32}{90}$	$\frac{7}{90}$		
5	$\frac{19}{288}$	$\frac{75}{288}$	$\frac{50}{288}$	$\frac{50}{288}$	$\frac{75}{288}$	$\frac{19}{288}$	
6	$\frac{41}{840}$	$\frac{216}{840}$	$\frac{27}{840}$	$\frac{272}{840}$	$\frac{27}{840}$	$\frac{216}{840}$	$\frac{41}{840}$

For the stiffness matrix:

$$K_{ij} = \int_{-1}^{+1}\int_{-1}^{+1}\int_{-1}^{+1} B_i D B_j \, \det J \, dr\,ds\,dt$$

where

$$G_{ij} = B_i D B_j \, \det J$$

and D is the constitutive matrix

The body force is given by:

$$F_{Bi} = \int_{-1}^{+1}\int_{-1}^{+1}\int_{-1}^{+1} H_i^T \, f_B \, \det J \, dr\,ds\,dt$$

where

$$G_i = H_i^T \, f_B \, \det J$$

and

$$[f_B]^T = [f_{Bx} \; F_{By} \; F_{Bz}]$$

The initial strain effect is given by:

$$F_{oi} = \int_{-1}^{+1}\int_{-1}^{+1}\int_{-1}^{+1} B_i D \varepsilon_o \, \det J \, dr\,ds\,dt$$

where

$$G_i = B_i D \; \varepsilon_o \, \det J$$

and

$$[\varepsilon_o]^T = [\varepsilon_x \; \varepsilon_y \; \varepsilon_z \; \gamma_{xy} \; \gamma_{yz} \; \gamma_{zx}]$$

The "consistent" mass matrix is given by:

$$M_{iJ} = \int_{-1}^{+1} \int_{-1}^{+1} \int_{-1}^{+1} \rho H_i^T H_j \det J \, dr\,ds\,dt$$

Where

$$G_{iJ} = \rho H_i^T H_J \det J$$

The thermal strain effect is given by:

$$F_{THi} = \int_{-1}^{+1} \int_{-1}^{+1} \int_{-1}^{+1} B_i^T D \varepsilon_{TH} \det J \, dr\,ds\,dt$$

Where

$$G_i = B_i^T D \varepsilon_{TH} \det J$$

And

$$[\varepsilon_{TH}]^T = [\alpha_x \Delta T \; \alpha_y \Delta T \; \alpha_z \Delta T \; 0 \; 0 \; 0]$$

The nonlinear strain effect is given by:

$$F_{NLi} = \int_{-1}^{+1} \int_{-1}^{+1} \int_{-1}^{+1} B_i^T \varepsilon_{NL} \det J \, dr\,s\,dt$$

Where

$$G_i = B_i^T D \varepsilon_{NL} \det J$$

And

$$[\varepsilon_{NL}]^T = [\varepsilon_{NLX} \; \varepsilon_{NLY} \; \varepsilon_{NLZ} \; \gamma_{NLXY} \; \gamma_{NLYZ} \; \gamma_{NLZX}]$$

The surface traction effect is given by:

$$F_{sri} = \int_{-1}^{+1} \int_{-1}^{+1} H_{si}^{T} \, f_s \, dA$$

Where the F_{sri} are the nodal forces due to surface tractions f_s on a surface of constant r. Similar expressions apply for surfaces of constant s or t.

$$dA = \begin{bmatrix} \frac{\partial x}{\partial s} \\ \frac{\partial y}{\partial s} \\ \frac{\partial z}{\partial s} \end{bmatrix} \times \begin{bmatrix} \frac{\partial x}{\partial t} \\ \frac{\partial y}{\partial t} \\ \frac{\partial z}{\partial t} \end{bmatrix} dsdt = \begin{bmatrix} \frac{\partial y}{\partial s}\frac{\partial z}{\partial t} - \frac{\partial z}{\partial s}\frac{\partial y}{\partial t} \\ \frac{\partial z}{\partial s}\frac{\partial x}{\partial t} - \frac{\partial x}{\partial s}\frac{\partial z}{\partial t} \\ \frac{\partial x}{\partial s}\frac{\partial y}{\partial t} - \frac{\partial y}{\partial s}\frac{\partial x}{\partial t} \end{bmatrix} dsdt$$

$$dA = Cdsdt$$

Then

$$Gi = H_{si}^{T} \, f_s \, C$$

Large Deflection Theory

Second order engineering strain-displacement equations

$$e_x = \frac{\partial u}{\partial x} + \frac{1}{2}\left[\left(\frac{\partial u}{\partial x}\right)^2 + \left(\frac{\partial v}{\partial x}\right)^2 + \left(\frac{\partial w}{\partial x}\right)^2\right]$$

$$e_y = \frac{\partial v}{\partial y} + \frac{1}{2}\left[\left(\frac{\partial u}{\partial y}\right)^2 + \left(\frac{\partial v}{\partial y}\right)^2 + \left(\frac{\partial w}{\partial y}\right)^2\right]$$

$$e_z = \frac{\partial w}{\partial z} + \frac{1}{2}\left[\left(\frac{\partial u}{\partial z}\right)^2 + \left(\frac{\partial v}{\partial z}\right)^2 + \left(\frac{\partial w}{\partial z}\right)^2\right]$$

$$e_{xy} = \frac{\partial u}{\partial y} + \frac{\partial v}{\partial x} + \left[\frac{\partial u}{\partial x}\frac{\partial u}{\partial y} + \frac{\partial v}{\partial x}\frac{\partial v}{\partial y} + \frac{\partial w}{\partial x}\frac{\partial w}{\partial y}\right]$$

$$e_{yz} = \frac{\partial v}{\partial z} + \frac{\partial w}{\partial y} + \left[\frac{\partial u}{\partial y}\frac{\partial u}{\partial z} + \frac{\partial v}{\partial y}\frac{\partial v}{\partial z} + \frac{\partial w}{\partial y}\frac{\partial w}{\partial z}\right]$$

$$e_{zx} = \frac{\partial w}{\partial x} + \frac{\partial u}{\partial z} + \left[\frac{\partial u}{\partial x}\frac{\partial u}{\partial z} + \frac{\partial v}{\partial x}\frac{\partial v}{\partial z} + \frac{\partial w}{\partial x}\frac{\partial w}{\partial z}\right]$$

$$[e] = [e_1] + [e_2]$$

$$\begin{bmatrix} e_{ix} \\ e_{iy} \\ e_{iz} \\ e_{ixy} \\ e_{iyz} \\ e_{izx} \end{bmatrix} = \begin{bmatrix} \frac{\partial u}{\partial x} \\ \frac{\partial v}{\partial y} \\ \frac{\partial w}{\partial z} \\ \frac{\partial v}{\partial z} + \frac{\partial w}{\partial y} \\ \frac{\partial w}{\partial x} + \frac{\partial u}{\partial z} \\ \frac{\partial u}{\partial y} + \frac{\partial v}{\partial x} \end{bmatrix}$$

$$[e_z] = \frac{1}{2} \begin{bmatrix} \frac{\partial u}{\partial x} & \frac{\partial v}{\partial x} & \frac{\partial w}{\partial x} & 0 & 0 & 0 & 0 & 0 & 0 \\ 0 & 0 & 0 & \frac{\partial u}{\partial y} & \frac{\partial v}{\partial y} & \frac{\partial x}{\partial y} & 0 & 0 & 0 \\ 0 & 0 & 0 & 0 & 0 & 0 & \frac{\partial u}{\partial z} & \frac{\partial v}{\partial w} & \frac{\partial w}{\partial z} \\ 0 & 0 & 0 & \frac{\partial u}{\partial z} & \frac{\partial v}{\partial z} & \frac{\partial w}{\partial z} & \frac{\partial u}{\partial y} & \frac{\partial v}{\partial y} & \frac{\partial w}{\partial y} \\ \frac{\partial u}{\partial z} & \frac{\partial v}{\partial z} & \frac{\partial w}{\partial z} & 0 & 0 & 0 & \frac{\partial u}{\partial x} & \frac{\partial v}{\partial x} & \frac{\partial w}{\partial x} \\ \frac{\partial u}{\partial y} & \frac{\partial v}{\partial y} & \frac{\partial w}{\partial y} & \frac{\partial u}{\partial x} & \frac{\partial v}{\partial x} & \frac{\partial w}{\partial x} & 0 & 0 & 0 \end{bmatrix} \begin{bmatrix} \frac{\partial u}{\partial x} \\ \frac{\partial v}{\partial x} \\ \frac{\partial w}{\partial x} \\ \frac{\partial u}{\partial y} \\ \frac{\partial v}{\partial y} \\ \frac{\partial w}{\partial y} \\ \frac{\partial u}{\partial z} \\ \frac{\partial v}{\partial z} \\ \frac{\partial w}{\partial z} \end{bmatrix}$$

Let

$$\left[d_x^1\right]^T = \left[\frac{\partial u}{\partial x} \frac{\partial v}{\partial x} \frac{\partial w}{\partial x}\right]$$

$$\left[d_y^1\right]^T = \left[\frac{\partial u}{\partial y} \frac{\partial v}{\partial y} \frac{\partial w}{\partial y}\right]$$

$$\left[d_z^1\right]^T = \left[\frac{\partial u}{\partial z} \frac{\partial v}{\partial z} \frac{\partial w}{\partial z}\right]$$

$$\left[d^1\right] = \begin{bmatrix} d_x^1 \\ d_y^1 \\ d_z^1 \end{bmatrix}$$

$$[A] = \begin{bmatrix} \left[d_x^1\right]^T & \left[0\right]^T & \left[0\right]^T \\ \left[0\right]^T & \left[d_y^1\right]^T & \left[0\right]^T \\ \left[0\right]^T & \left[0\right]^T & \left[d_z^1\right]^T \\ \left[0\right]^T & \left[d_z^1\right]^T & \left[d_y^1\right]^T \\ \left[d_z^1\right]^T & \left[0\right]^T & \left[d_x^1\right]^T \\ \left[d_y^1\right]^T & \left[d_x^1\right]^T & \left[0\right]^T \end{bmatrix}$$

Then,

$$\left[e_z \right] = \frac{1}{2} \, [A] \left[d^1 \right]$$

$$\Delta \left[e_z \right] = \frac{1}{2} \, \Delta \, [A] \left[d^1 \right] + \frac{1}{2} \, [A] \, \Delta \left[d^1 \right] = [A] \, \Delta \left[d^1 \right]$$

But,

$$\left[d^1 \right] = [G] \, [d]$$

$$[G] = \begin{bmatrix}
\frac{\partial H_1}{\partial x} & 0 & 0 & \frac{\partial H_2}{\partial x} & 0 & 0 & \cdots & \frac{\partial H_{20}}{\partial x} & 0 & 0 \\
0 & \frac{\partial H_1}{\partial x} & 0 & 0 & \frac{\partial H_2}{\partial x} & 0 & \cdots & 0 & \frac{\partial H_{20}}{\partial x} & 0 \\
0 & 0 & \frac{\partial H_1}{\partial x} & 0 & 0 & \frac{\partial H_1}{\partial x} & \cdots & 0 & 0 & \frac{\partial H_{20}}{\partial x} \\
\frac{\partial H_1}{\partial y} & 0 & 0 & \frac{\partial H_2}{\partial y} & 0 & 0 & \cdots & \frac{\partial H_{20}}{\partial y} & 0 & 0 \\
0 & \frac{\partial H_1}{\partial x} & 0 & 0 & \frac{\partial H_2}{\partial y} & 0 & \cdots & 0 & \frac{\partial H_{20}}{\partial y} & 0 \\
0 & 0 & \frac{\partial H_1}{\partial y} & 0 & 0 & \frac{\partial H_2}{\partial y} & \cdots & 0 & 0 & \frac{\partial H_{20}}{\partial y} \\
\frac{\partial H_1}{\partial z} & 0 & 0 & \frac{\partial H_2}{\partial z} & 0 & 0 & \cdots & \frac{\partial H_{20}}{\partial z} & 0 & 0 \\
0 & \frac{\partial H_1}{\partial z} & 0 & 0 & \frac{\partial H_2}{\partial z} & 0 & \cdots & 0 & \frac{\partial H_{20}}{\partial z} & 0 \\
0 & 0 & \frac{\partial H_1}{\partial z} & 0 & 0 & \frac{\partial H_2}{\partial z} & \cdots & 0 & 0 & \frac{\partial H_{20}}{\partial z}
\end{bmatrix}$$

So,

$$\Delta \left[d^1\right] = [A]\ \Delta\ \{[G]\ [d]\} = [A]\ [G]\ \Delta\ [d]$$

$$\Delta \left[d^1\right] = \left[B_2\right]\ \Delta\ [d]$$

$$\Delta\ [e] = \left[B_T\right]\ \Delta\ [d]$$

$$\left[B_T\right] = \left[B_1\right] + \left[B_2\right]$$

$$\left[B_2\right] = [A]\ [G]$$

The incremental stiffness is

$$[R] = \left[K_1\right] + \left[K_2\right] = \int_V [\bar{B}]^T\ [D]\ [\bar{B}]\ dV$$

$$\left[K_1\right] = \int_V \left[B_1\right]^T\ [D]\ \left[B_1\right]\ dV$$

$$\left[K_2\right] = \int_V \left(\left[B_1\right]^T\ [D]\ \left[B_2\right] + \left[B_2\right]^T\ [D]\ \left[B_2\right] + \left[B_2\right]^T\ [D]\ \left[B_1\right]\right)_{d_1}$$

The force unbalance is given by:

$$f(d) = \int_V [\bar{B}]\ [S]\ dV - [\bar{F}] = 0$$

Where

$[\bar{F}]$ are the applied forces

$$\Delta\ [e] = [\bar{B}]\ \Delta\ [d]$$

$$\Delta [f] = \int \Delta [\bar{B}]^T [S] \, dV + \int_V [\bar{B}]^T \Delta [S] \, dV$$

But

$$\Delta [\sigma] = [D] \Delta [e] = [D] [\bar{B}] \Delta [d]$$

And

$$\Delta [\bar{B}] = \Delta \left[B_2 \right]$$

Giving

$$\Delta [f] = \int_V \Delta \left[B_2 \right] [S] \, dV + \int_V [B]^T [D] [\bar{B}] \Delta [d]_{dV}$$

Defining

$$\left[K_S \right] \Delta [d] = \int_V \left[\bar{B}_2 \right]^T [S] \, dV$$

Gives

$$\Delta [f] = \left(\left[K_S \right] + \left[K_1 \right] \right) \Delta [d]$$

For eigenvalue problems:

$$\left(\left[K_1 \right] + \lambda \left[K_S \right] \right) \Delta [d] = 0$$

$$\left[B_2 \right]^T = [G]^T [A]^T$$

Then

$$\left[K_S \right] \Delta [d] = \int_V [G]^T \Delta [A]^T [S] \, dv$$

$$\Delta\,[A]^T\,[S] = \begin{bmatrix} S_x & 0 & 0 & S_{xy} & 0 & 0 & S_{xz} & 0 & 0 \\ 0 & S_x & 0 & 0 & S_{xy} & 0 & 0 & S_{xz} & 0 \\ 0 & 0 & S_x & 0 & 0 & S_{xy} & 0 & 0 & S_{xz} \\ S_{xy} & 0 & 0 & S_y & 0 & 0 & S_{yz} & 0 & 0 \\ 0 & S_{xy} & 0 & 0 & S_y & 0 & 0 & S_{yz} & 0 \\ 0 & 0 & S_{xy} & 0 & 0 & S_y & 0 & 0 & S_{yz} \\ S_{xz} & 0 & 0 & S_{yz} & 0 & 0 & S_z & 0 & 0 \\ 0 & S_{xz} & 0 & 0 & S_{yz} & 0 & 0 & S_z & 0 \\ 0 & 0 & S_{xz} & 0 & 0 & S_{yz} & 0 & 0 & S_z \end{bmatrix} \Delta \begin{bmatrix} d_x^1 \\ d_y^1 \\ d_z^1 \end{bmatrix}$$

$$= [M]\,\Delta\left[d^1\right]$$

But,

$$\Delta\left[d^1\right] = [G]\,\Delta\,[d]$$

Then

$$\left[K_S\right] = \int_v [G]^T\,[M]\,[G]\,dV$$

One of the major application areas for these graded material finite elements will involve small linear elastic strains but extremely large displacements. The severity of this condition is compounded by the involvement of temperature effects and body forces, conditions which have not been

extensively addressed. Additionally, eigenvalue/eigenvector analysis is required in the loaded conditions. We intend to take advantage of the significant improvements in computer speed and memory size in attacking this problem area.

We are using an incremental-updated Lagrangian approach. The virtual work equation for the updated Lagrangian formulation leads to the nonlinear incremental displacements from time (t) to time (t + Δt).

$$\int_{Vt}\left[C_{ijkl}\delta\Delta E_{kl}\Delta\varepsilon_{ij} - \frac{1}{2}\sigma_{ij}\delta\ 2\Delta\varepsilon_{ik}\Delta\varepsilon_{kj}\right. \tag{1}$$

$$\left. - \frac{\partial\Delta U_k}{\partial x_i}\frac{\partial\Delta U_k}{\partial x_j}\right] dV = \delta\overline{W}(t+\Delta t) - \int_{Vt}\sigma_{ij}\delta\Delta\varepsilon_{ij}dV$$

where

$$\delta\overline{W}(t+\Delta t) = \int_{Vt}(F_i + \Delta\overline{F}_i)\delta\Delta U_i dV \tag{2}$$

$$+ \int_{st}(T_i + \Delta\overline{T}_i)\delta\Delta U_i ds$$

$$\Delta\varepsilon_{ij} = \frac{1}{2}\left(\frac{\partial\Delta U_i}{\partial x_j} + \frac{\partial\Delta U_j}{\partial x_i}\right) \tag{3}$$

$\int_{Vt} C_{ijkl}\delta\Delta\varepsilon_{kl}\Delta\varepsilon_{ij}dV$ is equivalent to

$$\left[K_L\right]\left\{\Delta U^k\right\} = \left(\int_{Vt}\left[B_L\right]^T[C]\left[B_L\right]dV\right)\left\{\Delta U^k\right\} \tag{4}$$

$-2\int_{Vt}\sigma_{ij}\delta\Delta\varepsilon_{ik}\Delta\varepsilon_{kj}dV$ is equivalent to

$$[K_{N1}]\ \{\Delta U^k\} = \left(\int_{Vt} [B_L]^T\ [\sigma_1]\ [B_L]\ dV\right)\{\Delta U^k\} \tag{5}$$

$\int_{Vt} \sigma_{ij}\delta\Delta U_{k,i}\cdot\Delta U_{k,j}dV$ is equivalent to

$$[K_{N2}]\ \{\Delta U^k\} = \left(\int_{Vt} [B_2]^T\ [\sigma_2]\ [B_2]\ dV\right)\{\Delta U^k\} \tag{6}$$

and

$\int_{Vt} \sigma_{ij}\delta\Delta\varepsilon_{ij}dV$ is equivalent to

$$\int_{Vt}[B_L]^T\{\sigma\}dV \tag{7}$$

where

$$\{\Delta\varepsilon\} = [B_L]\{\Delta U^k\} \tag{8}$$

$$\{\Delta U\}_{ij} = [B_2]\{\Delta U^k\} \tag{9}$$

$$\{\Delta U\}_{ij} = [\Delta U_{1,1}\ \Delta U_{1,2}\ \cdots\cdots\ \Delta U_{3,3}]^T \tag{10}$$

$$\{\Delta U^k\} = [\ldots\Delta u_1^k\ \Delta u_2^k\ \Delta u_3^k\ldots]^T \tag{11}$$

The incremental equilibrium is

$$\left([K_L] + [K_N]\right)\{\Delta U^k\} = \{\Delta P\} \tag{12}$$

where

$[K_1]$ is the linear stiffness matrix, i.e.

$$[K_L] = \int_{Vt}[B_L]^T\ [C]\ [B_L]\ dV \tag{13}$$

$[K_N]$ is the nonlinear stiffness matrix due to larger deformation, i.e.

$$[K_N] = [K_{N1}] + [K_{N2}] \tag{14}$$

$$[K_{N1}] = \int_{Vt} [B_L]^T [\sigma_1] [B_L] \, dV \tag{15}$$

$$[K_{N2}] = \int_{Vt} [B_2]^T [\sigma_2] [B_2] \, dV \tag{16}$$

$\{\Delta P\}$ is the incremental load from time (t) to (t + Δt) i.e.

$$\{\Delta P\} = R(t + \Delta t) - \int_{Vt} [B_L]^T \{\sigma\} \, dV \tag{17}$$

The stress matrices are given by

$$[\sigma_2] = \begin{bmatrix} [\bar{\sigma}] & 0 & 0 \\ 0 & [\bar{\sigma}] & 0 \\ 0 & 0 & [\bar{\sigma}] \end{bmatrix} \tag{18}$$

$$[\bar{\sigma}] = \begin{bmatrix} \sigma_{11} & \sigma_{12} & \sigma_{13} \\ \sigma_{12} & \sigma_{22} & \sigma_{23} \\ \sigma_{13} & \sigma_{23} & \sigma_{33} \end{bmatrix} \tag{19}$$

$$[\sigma_1] = \begin{bmatrix} -2\sigma_{11} & 0 & 0 & -\sigma_{12} & 0 & -\sigma_{13} \\ & -2\sigma_{22} & 0 & -\sigma_{12} & -\sigma_{23} & 0 \\ & & -2\sigma_{33} & 0 & -\sigma_{23} & -\sigma_{13} \\ & & & -\frac{1}{2}(\sigma_{11}+\sigma_{22}) & -\frac{1}{2}\sigma_{13} & -\frac{1}{2}\sigma_{23} \\ & \text{(Symmetric)} & & & -\frac{1}{2}(\sigma_{22}+\sigma_{33}) & -\frac{1}{2}\sigma_{12} \\ & & & & & -\frac{1}{2}(\sigma_{33}+\sigma_{11}) \end{bmatrix} \tag{20}$$

Eigenvalue/Eigenvector Analysis

We are developing the algorithms for solving the lowest eigenvalue and eigenvector pairs for large structure system of equations; that is,

$$K\phi_i = \lambda_i M\phi_i$$

where

K is the maximum symmetric stiffness matrix

M is the maximum symmetric mass matrix

λ_i is the ith eigenvalue

ϕ_i is the ith eigenvector

The methodologies coded so far are the determinant search and subspace iteration techniques.

Both of these techniques have been investigated extensively in a finite element code that uses 8-noded shell elements and the COLSOL solution scheme. The addition of the eigenvalue/eigenvector analysis capability is closely linked to the solution procedure, and extensive changes to the COLSOL routines were required. Both lumped mass and consistent mass matrices were coded.

Determinant Search Method

In the determinant-search technique, a Sturm sequence check is very useful for estimating the proper eigenshift. Once the proper eigenshift is located in the neighborhood of the desired eigenvalue, a Rayleigh-quotient is then employed to iterate the trial vector until convergence is reached. A valid starting trial vector should be used, otherwise it may converge to the wrong result even though the proper eigenvalue is obtained in the repeated roots case. The logics for determining the proper eigenshift requires eigen deflation, Gram-Schmidt orthogonality if necessary, and schemes of acceleration, bisection, secant, or quadratic solutions. Appendix B shows the test case results of this procedure.

Subspace Iteration

The subspace iteration technique employs vector transformation into smaller q ($n \leqq q \leqq m$) eigen spaces, that is

The transformation matrix [x] is obtained through the successive inverse iteration process,

$$[K]\ [x]_{k+1} = [m]\ [x]_k$$

where k is the iteration number. After transformation, the large eigenvalue problem is reduced to the small eigenvalue system containing the q eigenpairs and is easily solved by the well-known Jacobi rotation technique, that is

$$[\bar{K}]\ [\bar{v}] = [\bar{m}]\ [\bar{v}]\ [\bar{\lambda}]$$

where

$$[\bar{K}] = [\bar{x}]^T\ [K]\ [\bar{x}]$$

$$[\bar{m}] = [\bar{x}]^T\ [m]\ [\bar{x}]$$

$[\bar{x}]$ = q × q diagonal eigenvalue matrix

$[\bar{v}]$ = q × q eigenvector matrix corresponding $[\lambda]$

Even though these methodologies have been widely used, the solution accuracy as well as economy rely heavily on the actual numerical implementation. The following numerical considerations are being kept in mind during program development.

1. Scale-Factors

   a. The mass value is, in general, much smaller than the stiffness value. A reasonable scale factor (10^6 for instance) should be imposed on the mass matrix in order to minimize numerical truncation errors.

   b. The determinant of the matrix [K - M] is, in general, very large. Care will be taken to avoid numerical overflow.

2. Numerical Precision

   Depending on the computer hardware, double precision or even quadruple precision may be necessary.

3. Starting Trial Eigenvector

The starting trial eigenvector significantly affects the iteration convergence rate. Most important is that the wrong trial eigenvector may lead to the wrong solution in the determinant search technique. In the subspace iteration technique, improper trial eigenvectors may skip some eigenpairs.

4. Convergence Criteria Limits

a. Maximum number of iterations

b. Rayleigh-Quotient iteration tolerance

c. Eigenvector iteration tolerance

d. Solution convergence error tolerance

5. The eigenshift for determinant search Rayleigh-quotient iteration technique may converge to the wrong result if the proper eigenshift is not determined. In order to determine the proper eigenshift for the next eigenvalue, techniques should be investigated in order to minimize the number of large matrix decompositions.

6. Efficient decomposition and back substitution matrix decomposition and back substitution play the most important role in the cost of performing eigenvalue analysis.

Heat Transfer Development

Linear steady-state Equation:

at time step: $t + \Delta t$:

$$\int \bar{\theta}^{,t}{}_k \, {}^{t+\Delta t}\theta' \, dr + \int_{sc} \bar{\theta}^s \, h \, {}^{t+\Delta t}\theta^s \, ds$$

$$= {}^{t+\Delta t}Q_e + \int_{sc} \bar{\theta}^s \, h \, {}^{t+\Delta t}\theta_e \, ds$$

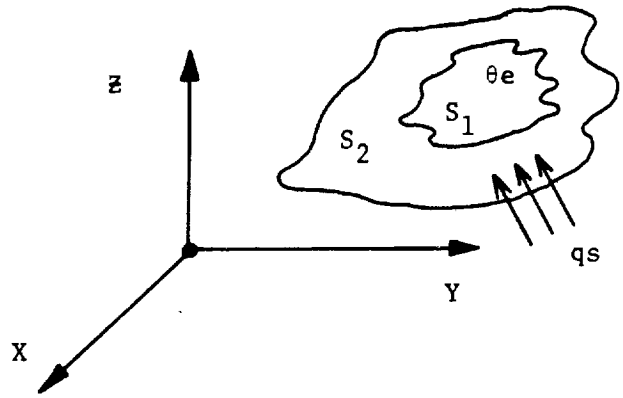

where $\theta^{,t} = \begin{bmatrix} \frac{\partial\theta}{\partial x} & \frac{\partial\theta}{\partial y} & \frac{\partial\theta}{\partial z} \end{bmatrix}$

$$K = \begin{bmatrix} K_x & 0 & 0 \\ 0 & K_y & 0 \\ 0 & 0 & K_z \end{bmatrix}$$

h = convection coefficient

s = surface of the body

governing equation: Linear heat transfer

$$(K^K + K^C)\, Q_{t+\Delta t} = Q_{t+\Delta t} + Q^e_{t+\Delta t} \qquad (A)$$

where K^K - the conductivity matrix

$$K^K = \sum_{m=1}^{m} \int_{Vm} B^{m\,t} \cdot K^m B^m \, dV_m \qquad (I)$$

K^C - the convection matrix

$$K^C = \sum_{m=1}^{m} \int_{SC^m} h^{(m)} \cdot H^{s(m)^T} H^{s(m)} \cdot ds^{(m)} \qquad (II)$$

the nodal point heat flow input vector $Q_{(t+\Delta t)}$

$$Q_{t+\Delta t} = Q_{B(t+\Delta t)} + Q_{S(t+\Delta t)} + Q_{C(t+\Delta t)} \qquad (B)$$

where $Q_{B\,t+\Delta t} = \sum_{m} \int_{vm} H^{(m)^T} \cdot q^{b(m)}_{t+\Delta t} \, dV^m \qquad (III)$

$$Q_{S(t+\Delta t)} = \sum_{m} \int_{s_2 (m)} H^{S(m)^T} q^{S(m)}_{t+\Delta t} \cdot ds^{(m)} \qquad (IV)$$

where $Q_{C(t+\Delta t)}$ - a vector of concentrated nodal point heat flow input

The nodal point heat flow contribution $Q^{e}_{t+\Delta t}$ is due to the convection boundary condition

$\underline{q}^{b}$ - the rate of heat generated in element

$\underline{q}^{s}$ - the surface heat flow input

At that time:

$$\theta^{(e)}_{t+\Delta t} = H^{(e)} \cdot \theta_{t+\Delta t} \qquad (1a)$$

$$\theta^{s(e)}_{t+\Delta t} = H^{s(e)}\, \theta_{t+\Delta t} \qquad (1b)$$

$$\theta^{(e)}_{t+\Delta t} = B^{(e)} \cdot \theta_{t+\Delta t} \qquad (1c)$$

where (e) $\longrightarrow$ denotes element m

$\theta_{t+\Delta t} \longrightarrow$ a vector of all nodal point temperatures at $t+\Delta t$

$$\theta^{T}_{t+\Delta t} = \left[\theta_{1}{}^{t+\Delta t} \quad \theta_{2}{}^{t+\Delta t} \quad \theta_{3}{}^{t+\Delta t} \text{ ------ } \theta_{m}{}^{t+\Delta t} \right]$$

The matrix $H^{(e)} \longrightarrow$ Element Temperature

$B^{(e)} \longrightarrow$ Temperature gradient interpolation matrice

$H^{s(e)} \longrightarrow$ The surface temperature interpolation matrix

[B] ⟶ derivative of the shape function with respect to r, s, t and pre-multiplication by J^{-1}

$$Q^{e}_{t+\Delta t} = \sum_{m} \int_{sc(m)} h \cdot H^{s(m)^T} \cdot H^{s(m)} \cdot \theta_e(t+\Delta t) \cdot dS^{(m)} \qquad (V)$$

$\theta_{e\ t+\Delta t}$ The given nodal point environmental temperatures.

from this equation to find the $Q^{e}_{t+\Delta t}$ (i.e. $\theta_{e\ t+\Delta t}$ and h are given)

Shape Function:

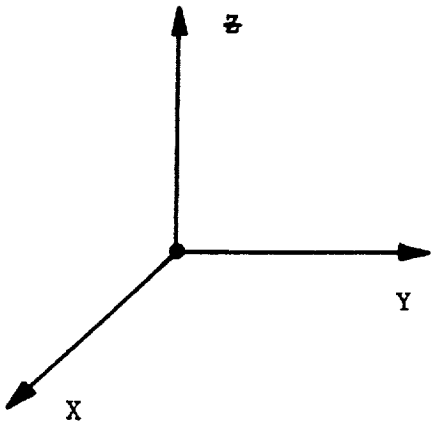

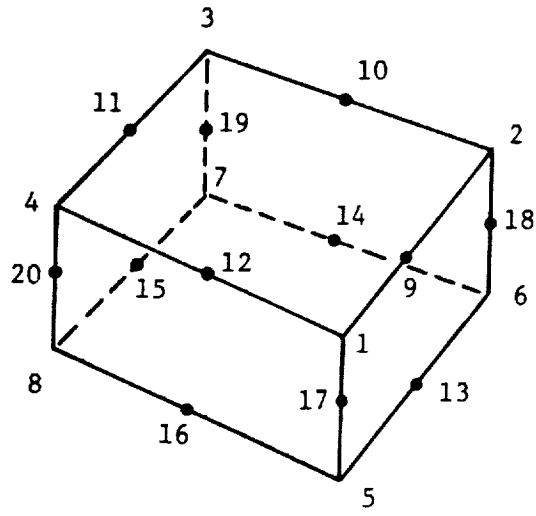

$$H_1 = g_1 - (g_9 + g_{12} + g_{17})/2$$

$$H_2 = g_2 - (g_9 + g_{10} + g_{18})/2$$

$$H_3 = g_3 - (g_{10} + g_{11} + g_{19})/2$$

$$H_4 = g_4 - (g_{11} + g_{12} + g_{20})/2$$

$$H_5 = g_5 - (g_{13} + g_{16} + g_{17})/2$$

$$H_6 = g_6 - (g_{13} + g_{14} + g_{18})/2$$

$$H_7 = g_7 - (g_{14} + g_{15} + g_{19})/2$$

$$H_8 = g_8 - (g_{15} + g_{16} + g_{20})/2$$

$H_i = g_i$ for (i = 9 .... 20)

g_i = 0 if node i is not includes; otherwise:

$g_i = G(r, r_i)\ G(s, s_i)\ G(t, t_i)$

$G(\beta, \beta_i) = 1/2\ (1+\beta_i\beta)$ for $\beta_i = \pm 1$

$G(\beta,\beta_i) = (1-\beta^2)$ for $\beta_i = 0$

Jacobi's operator [J] is

The displacement functions:

$X = \Sigma\ H_i x_i$

$Y = \Sigma\ H_i y_i$

$Z = \Sigma\ H_i z_i$

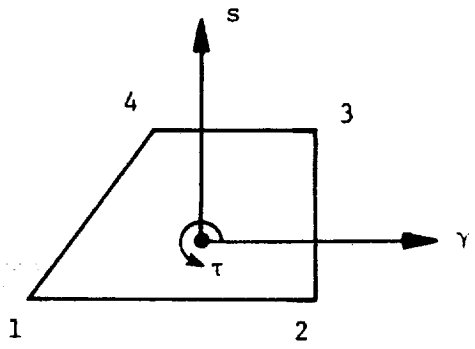

$$[J] = \begin{bmatrix} \frac{\partial x}{\partial r} & \frac{\partial y}{\partial r} & \frac{\partial z}{\partial r} \\ \frac{\partial x}{\partial s} & \frac{\partial y}{\partial s} & \frac{\partial z}{\partial s} \\ \frac{\partial x}{\partial t} & \frac{\partial y}{\partial t} & \frac{\partial z}{\partial t} \end{bmatrix}$$

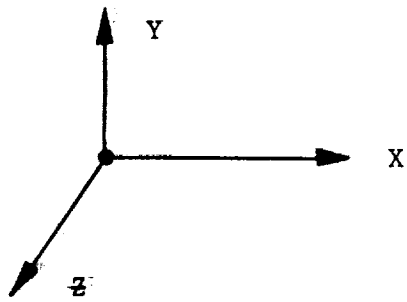

where r, s, t are the local coordinates.

$$[B] = [J] \begin{bmatrix} \frac{\partial H_1}{\partial r} & \cdots & \frac{\partial H_i}{\partial r} \\ \frac{\partial H_1}{\partial s} & \cdots & \frac{\partial H_i}{\partial s} \\ \frac{\partial H_1}{\partial t} & \cdots & \frac{\partial H_i}{\partial t} \end{bmatrix}$$

$\underline{q}^b$ - the rate of heat generated per unit volume

θ_e - the environmental temperature

$\underline{q}^s$ - the heat flow input to the surface of the body

h - the convection coefficient

$$q^s = h(\theta_e - \theta^s)$$

θ - is the temperature of the body

$$\left\{\begin{array}{l} \theta^{(m)}_{t+\Delta t} = H^{(m)}\,\theta_{t+\Delta t} \\ \theta^{s(m)} = H^{s(m)}\theta_{t+\Delta t} \\ \theta^{\cdot(m)} = B^{(m)}\cdot\,\theta_{t+\Delta t} \end{array}\right\} \qquad \theta_{t+\Delta t} \text{ - a vector of all nodal point temperatures at } t+\Delta t$$

$$\theta^{T}_{t+\Delta t} = [\theta_{1\,t+\Delta t}\ \theta_2 \quad \theta_m]_{t+\Delta t}$$

a): from Equations (I), (II) we can find the

$(K^k$ & $K^c)$

(b): From Equation (B) the nodal point heat flow input

$$Q_{t+\Delta t} = Q_{B(t+\Delta t)} + Q_{S(t+\Delta t)} + Q_{C(t+\Delta t)}$$

where

$$\left\{\begin{array}{l} Q_{B(t+\Delta t)} = \sum_m \int_{vm} H(m)^T \; q^{b(m)}_{(t+\Delta t)}\; dV^{(m)} \\ Q_{s(t+\Delta t)} = \sum_m \int_{S2} H^{s(m)^T} \cdot \; q^{s(m)}_{(t+\Delta t)}\; dS^{(m)} \end{array}\right.$$

$Q_{c(t+\Delta t)}$ - a vector of concentrated nodal point heat flow input

It can be solved for $Q_{(t+\Delta t)}$

(c): From Equation (V) the given nodal point environment temperatures

$\theta_{e(t+\Delta t)}$

$$Q^{e}_{(t+\Delta t)} = \sum_{m} \int_{sc} h \cdot H^{s(m)^{T}} \cdot H^{s(m)} \cdot \Theta_{e(t+\Delta t)} \, dS^{(m)}$$

can solve for $Q^{e}_{(t+\Delta t)}$ (nodal point heat distribution)

From items (a), (b), (c), substitute into Equation A.

$$(K^{k} + K^{c}) \, \Theta_{(t+\Delta t)} = Q_{(t+\Delta t)} + Q^{e}_{(t+\Delta t)}$$

The nodal point temperatures in each element can be found by using equations (1a), (1b), (1c).

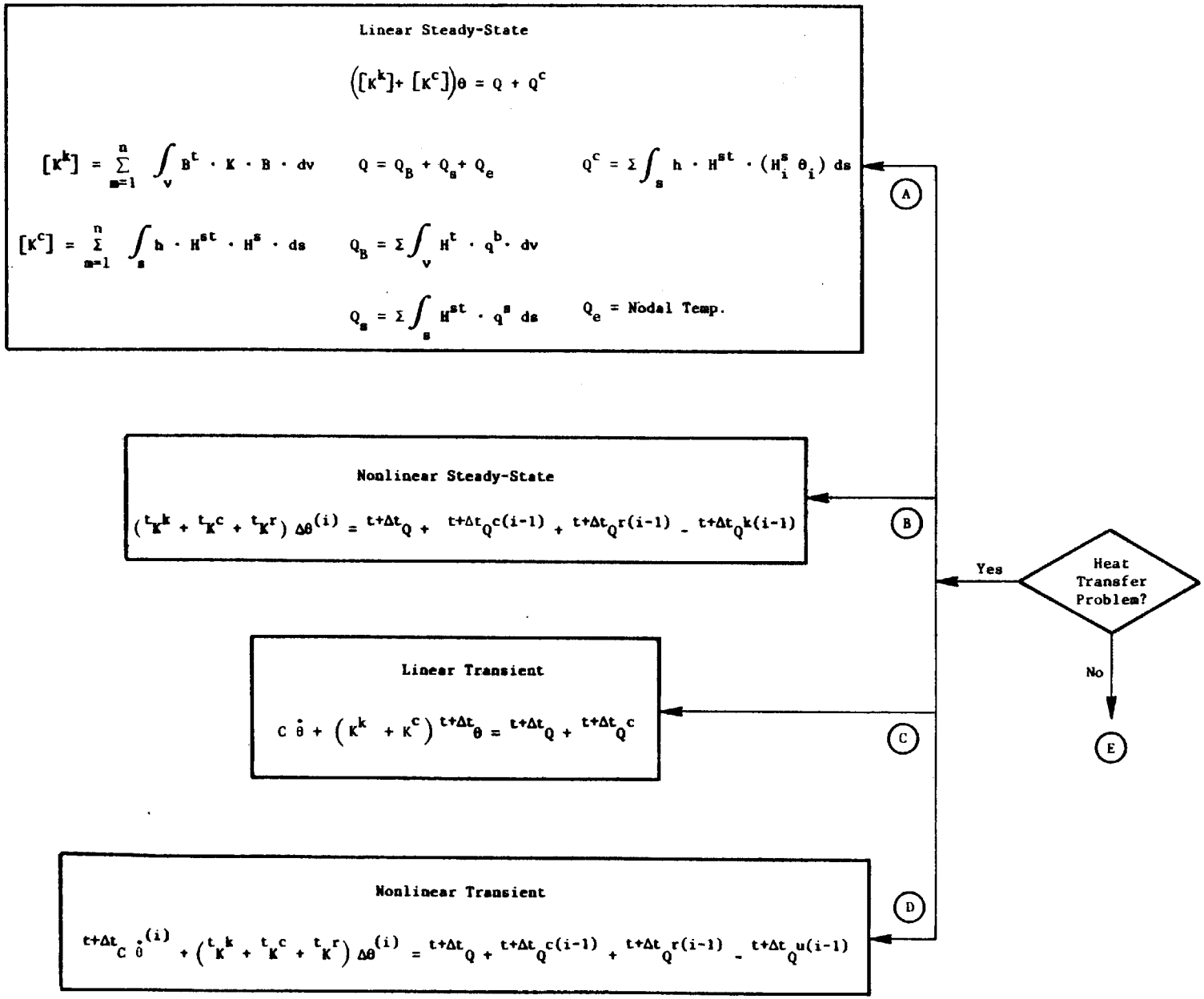
Linear Steady-State
$\left([K^k]+[K^c]\right)\theta = Q + Q^c$
$[K^k] = \sum_{m=1}^{n} \int_v B^t \cdot K \cdot B \cdot dv$
$Q = Q_B + Q_s + Q_e$
$Q^c = \Sigma \int_s h \cdot H^{st} \cdot (H_i^s \theta_i)\, ds$
$[K^c] = \sum_{m=1}^{n} \int_s h \cdot H^{st} \cdot H^s \cdot ds$
$Q_B = \Sigma \int_v H^t \cdot q^b \cdot dv$
$Q_s = \Sigma \int_s H^{st} \cdot q^s\, ds$
Q_e = Nodal Temp.
A
Nonlinear Steady-State
$({}_tK^k + {}_tK^c + {}_tK^r)\,\Delta\theta^{(i)} = {}^{t+\Delta t}Q + {}^{t+\Delta t}Q^{c(i-1)} + {}^{t+\Delta t}Q^{r(i-1)} - {}^{t+\Delta t}Q^{k(i-1)}$
B
Yes
Heat Transfer Problem?
No
E
Linear Transient
$C\,\dot{\theta} + \left(K^k + K^c\right)^{t+\Delta t}\theta = {}^{t+\Delta t}Q + {}^{t+\Delta t}Q^c$
C
Nonlinear Transient
${}^{t+\Delta t}C\,\dot{\theta}^{(i)} + \left({}_tK^k + {}_tK^c + {}_tK^r\right)\Delta\theta^{(i)} = {}^{t+\Delta t}Q + {}^{t+\Delta t}Q^{c(i-1)} + {}^{t+\Delta t}Q^{r(i-1)} - {}^{t+\Delta t}Q^{u(i-1)}$
D

A. Linear Steady-State:

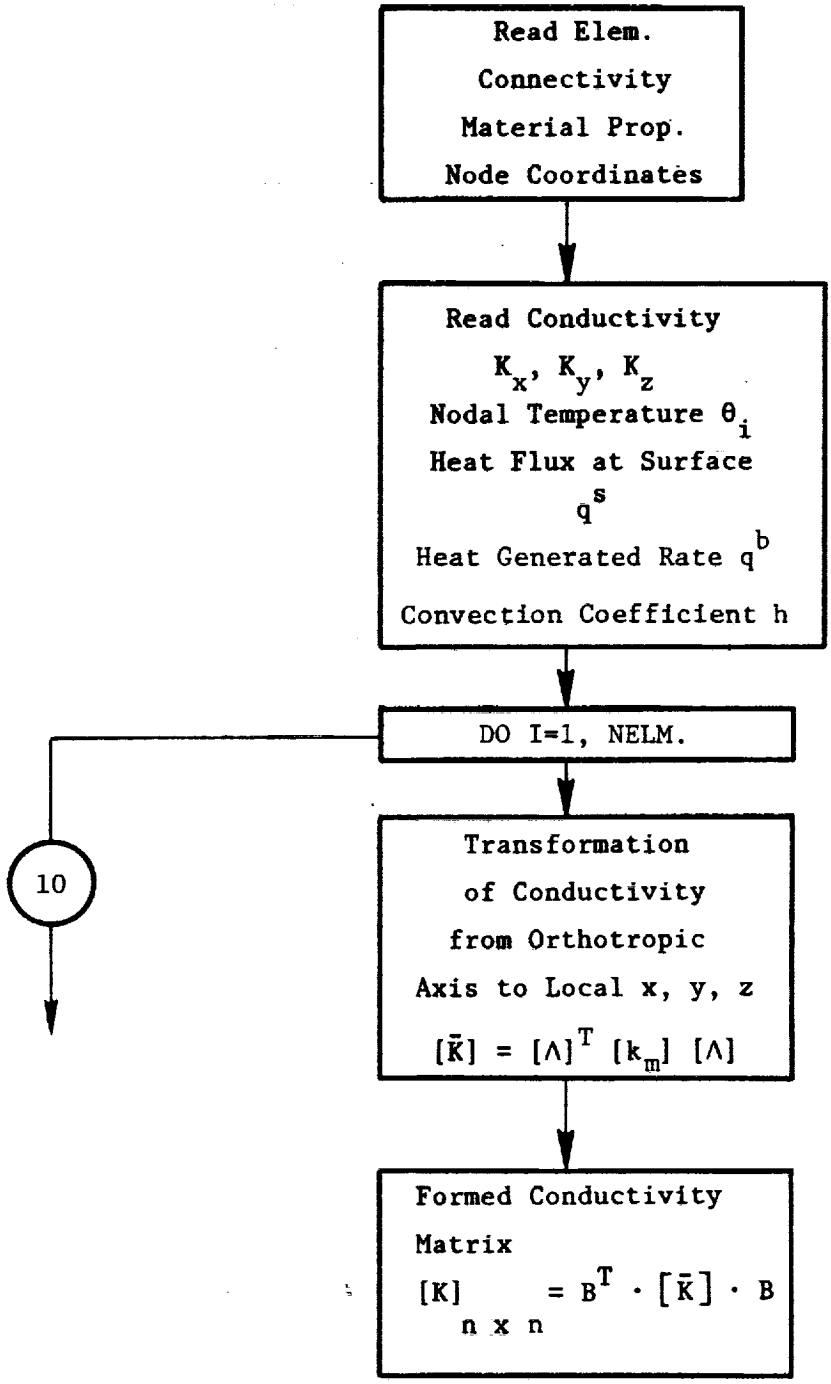

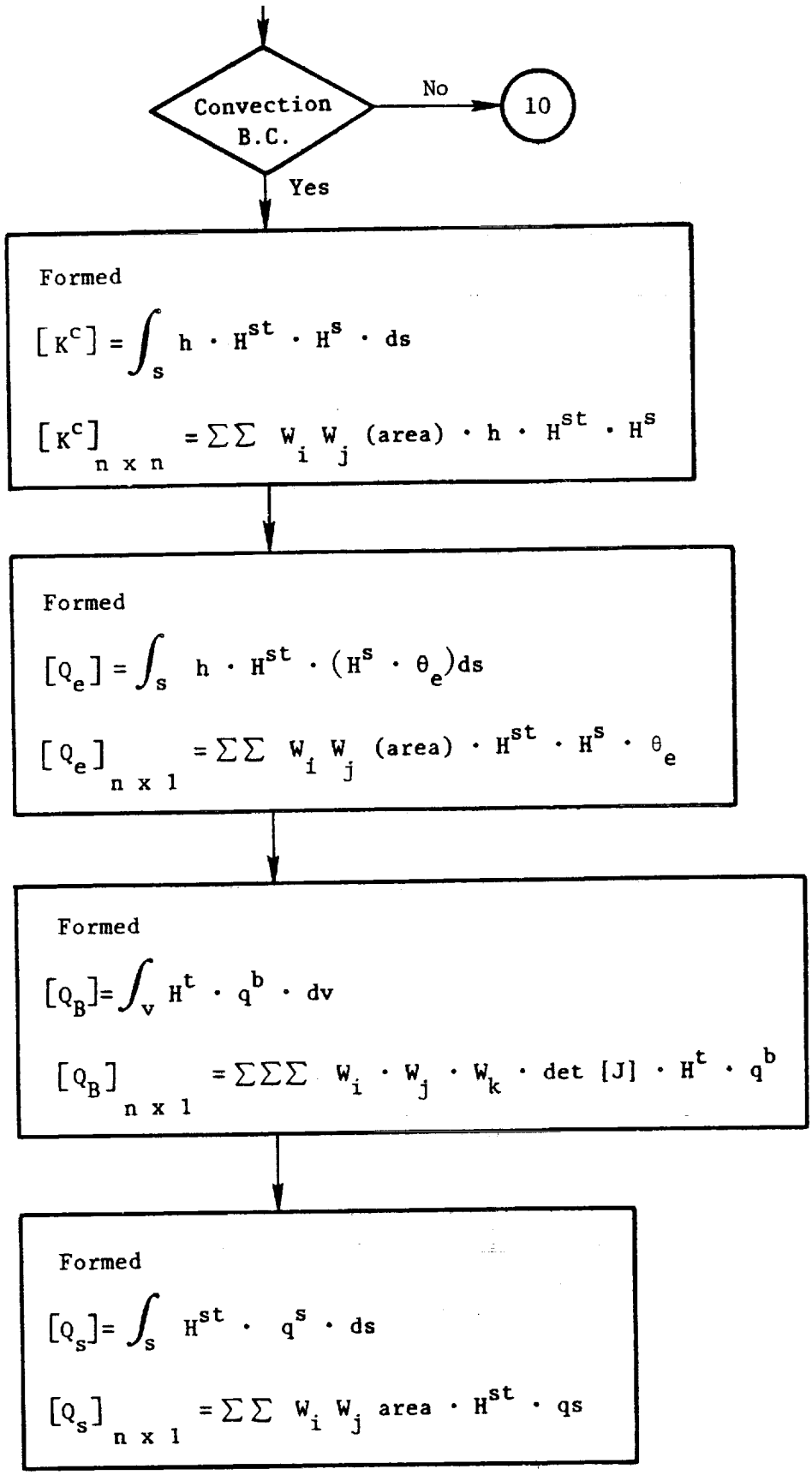
Convection B.C.
No
10
Yes
Formed
$[K^c] = \int_s h \cdot H^{st} \cdot H^s \cdot ds$
$[K^c]_{n \times n} = \sum\sum W_i W_j (\text{area}) \cdot h \cdot H^{st} \cdot H^s$
Formed
$[Q_e] = \int_s h \cdot H^{st} \cdot (H^s \cdot \theta_e) ds$
$[Q_e]_{n \times 1} = \sum\sum W_i W_j (\text{area}) \cdot H^{st} \cdot H^s \cdot \theta_e$
Formed
$[Q_B] = \int_v H^t \cdot q^b \cdot dv$
$[Q_B]_{n \times 1} = \sum\sum\sum W_i \cdot W_j \cdot W_k \cdot \det [J] \cdot H^t \cdot q^b$
Formed
$[Q_s] = \int_s H^{st} \cdot q^s \cdot ds$
$[Q_s]_{n \times 1} = \sum\sum W_i W_j \text{ area} \cdot H^{st} \cdot qs$

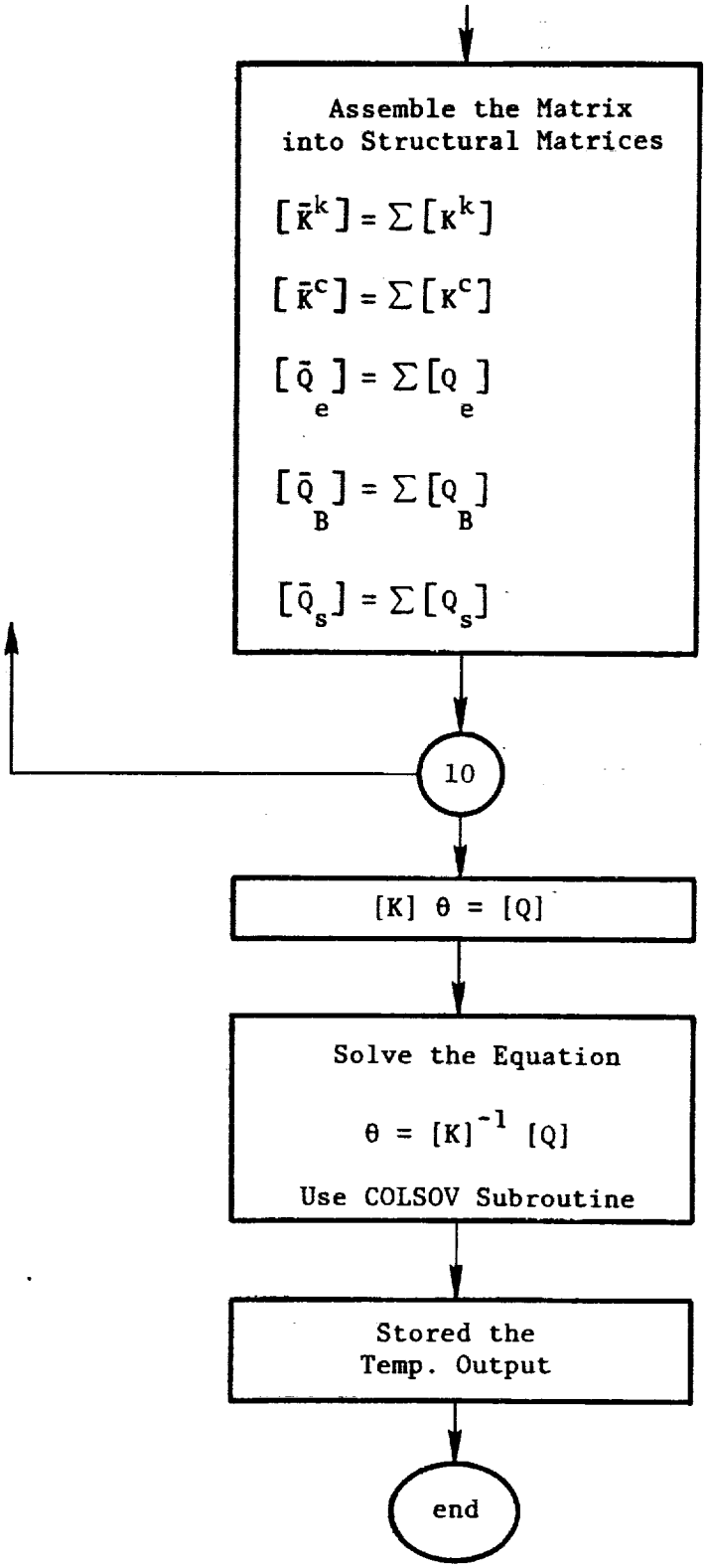
Assemble the Matrix into Structural Matrices
$[\bar{K}^k] = \Sigma [K^k]$
$[\bar{K}^c] = \Sigma [K^c]$
$[\bar{Q}_e] = \Sigma [Q_e]$
$[\bar{Q}_B] = \Sigma [Q_B]$
$[\bar{Q}_s] = \Sigma [Q_s]$
10
[K] θ = [Q]
Solve the Equation
$\theta = [K]^{-1} [Q]$
Use COLSOV Subroutine
Stored the Temp. Output
end

3D Magnetic-Field Problems - The general governing equations are:

$$\begin{cases} \nabla \times \vec{H} = \vec{J} & (1) \\ \vec{B} = \mu \vec{H} & (2) \\ \nabla \cdot \vec{B} = 0 & (3) \end{cases}$$

where $\vec{H}$, $\vec{B}$, and $\vec{J}$ are vector quantities (with three space components);

$\vec{H}$ = the magnetic-field strength,

$\vec{B}$ = the magnetic-flux density, (Only $\vec{J}$ is a prescribed quantity; $\vec{H}$ and $\vec{B}$ represent six unknown variables.)

and $\vec{J}$ = the magnetic-current density;

μ = the magnetic permeability;

and $\nabla = \left[\frac{\partial}{\partial x} \vec{i} + \frac{\partial}{\partial y} \vec{j} + \frac{\partial}{\partial z} \vec{k} \right]$.

Define $\vec{B} = \nabla \times \vec{A}$, where $\vec{A}$ is a vector potential; then:

$$\nabla \cdot \vec{B} = \nabla \cdot (\nabla \times \vec{A}) = 0$$

$$\therefore \quad \nabla \times \vec{H} = \nabla \times \frac{\vec{B}}{\mu} = \nabla \times \frac{1}{\mu} \nabla \times \vec{A} = \vec{J}$$

$$\therefore \quad \nabla \times \frac{1}{\mu} \nabla \times \vec{A} = \vec{J} \qquad (4)$$

This equation is equivalent to a stationarity of a variational functional II, defined as

$$II = \tfrac{1}{2} \int_v \vec{A}^T \nabla \times \frac{1}{\mu} \nabla \times \vec{A} \, dv - \int_v \vec{A}^T \vec{J} \, dv \qquad (5)$$

where $\vec{A} = \sum_{i=1}^{n} N_i a_i$

N_i = shape function of x, y, z

$N_i = N_i(x, y, z)$

a_i = the nodal value at Node i

$a_i = a_i(t)$

where v is all space.

Define $H = \vec{H}_s + \vec{H}_m$ where

$\vec{H}_s$ = the magnetic source field,

and $\vec{H}_m$ = the induced magentizations.

The $\vec{H}_s$ is any vector defined such that

$$\nabla \times \vec{H}_s = \vec{J} \tag{6}$$

then Equation 1 becomes:

$$\nabla \times \vec{H}_m = 0 \tag{7}$$

This can be identically satisfied by introducing a scalar potential ϕ defined by:

$$\vec{H}_m = -\nabla\phi \tag{8}$$

Eliminating $\vec{B}$ from Equations 2 and 3:

$$\nabla \cdot \vec{B} = \nabla \cdot \mu\vec{H} = \nabla \cdot \mu(\vec{H}_s + \vec{H}_m) = 0$$

$$\therefore \quad -\nabla \cdot \mu\nabla\phi + \nabla \cdot \mu\vec{H}_s = 0 \tag{9}$$

For a simple scalar unknown ϕ

$$\phi = \Sigma N_i a_i$$

where
$$\begin{cases} \phi = \phi\ (x, y, z, t) \\ N_i = N_i\ (x, y, z) \\ a_i = a_i\ (t) \end{cases}$$

Equation 9 may be written

$$\nabla \cdot \mu \nabla \phi = \frac{\partial}{\partial x}\left(\mu_x \frac{\partial \phi}{\partial x}\right) + \frac{\partial}{\partial y}\left(\mu_y \frac{\partial \phi}{\partial y}\right) + \frac{\partial}{\partial z}\left(\mu_z \frac{\partial \phi}{\partial z}\right) \tag{10}$$

and, with the known quantity, written as:

$$f = \nabla \cdot \mu \cdot \vec{H}_s \tag{11}$$

For steady-state (time-dependent) problems, Equations 10 and 11 may be rewritten:

$$\frac{\partial}{\partial x}\left(\mu_x \frac{\partial \phi}{\partial x}\right) + \frac{\partial}{\partial y}\left(\mu_y \frac{\partial \phi}{\partial y}\right) + \frac{\partial}{\partial z}\left(\mu_z \frac{\partial \phi}{\partial z}\right) = f(x, y, z) \tag{12}$$

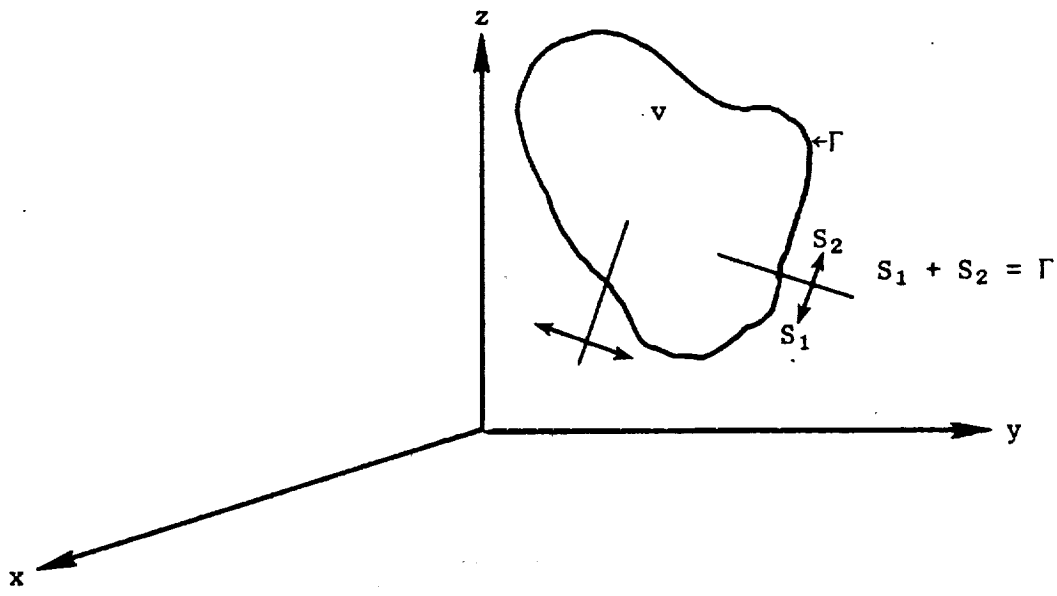

Boundary Conditions - Equation 12 is general and must be solved subject to additional constraints on the boundary surface. On S_1, if nonlinear $\phi = \phi\ (x, y, z, t)$,

$$\phi = \phi\ (x, y, z) \tag{13}$$

while the remaining part of the boundary has the following condition on S_2

$$\mu_x \frac{\partial \phi}{\partial x} n_x + \mu_y \frac{\partial \phi}{\partial y} n_y + \mu_z \frac{\partial \phi}{\partial z} n_z + g\ (x, y, z) = 0 \tag{14}$$

where n_x, n_y, and n_z are the direction cosines of the outward normal of the surface, and the union S_1 and S_2 forms the complete boundary Γ, $(S_1 + S_2 = \Gamma)$. Equation 13 is called Dirichlet condition, and Equation 14 is called Cauchy boundary condition; if $g = 0$, it is called Neumann boundary condition. A field problem is said to have mixed boundary conditions when some portions of Γ have Dirichlet while others have Cauchy.

In Equation 12, if $\mu_x = \mu_y = \mu_z$ = constant = μ, $\nabla^2\phi = f(x, y, z)/\mu$ is called Poisson's equation. If $f = 0$, then $\nabla^2\phi = 0$ is known as the Laplace equation.

Variational Principal - The function $\phi(x, y, z)$ that satisfies Equations 12, 13, and 14 also minimizes the functional:

$$I(\phi) = \tfrac{1}{2} \int_v [\mu_x (\frac{\partial \phi}{\partial x})^2 + \mu_y (\frac{\partial \phi}{\partial y})^2 + \mu_z (\frac{\partial \phi}{\partial z})^2 + 2f\phi]\ dxdydz + \int_{S_2} (g\phi)\ dS_2 \tag{15}$$

$$\delta I(\phi) = 0 \tag{16}$$

Element Equations - Suppose that the solution domain v is divided into M elements of γ nodes each. In each element, the unknown function may be expressed by

$$\phi^{(e)} = \sum_{i=1}^{\gamma} N_i \phi_i = [N]\{\phi\}^{(e)} \tag{17}$$

where ϕ_i is the nodal value of ϕ at Node i. Equation 17 implies that only nodal values of ϕ are taken as nodal degrees of freedom, but derivatives of ϕ may also be used as nodal parameters.

$$I(\phi) = \sum_{e=1}^{n} I(\phi^{(e)})$$

$$\therefore \quad \frac{\partial I(\phi^{(e)})}{\partial \phi_i} = 0, \qquad i = 1, 2, \ldots . \gamma$$

For a Node i on boundary S_2, from Equation 15 we have on Surface $S_2^{(e)}$:

$$\frac{\partial I(\phi^{(e)})}{\partial \phi_i} =$$

$$\int_{v^{(e)}} [\mu_x \frac{\partial \phi^{(e)}}{\partial x} \frac{\partial}{\partial \phi_i} (\frac{\partial \phi^{(e)}}{\partial x}) + \mu_y \frac{\partial \phi^{(e)}}{\partial y} \frac{\partial}{\partial \phi_i} (\frac{\partial \phi^{(e)}}{\partial y}) + \mu_z \frac{\partial \phi^{(e)}}{\partial z} \frac{\partial}{\partial \phi_i} (\frac{\partial \phi^{(e)}}{\partial z})$$

$$+ f \frac{\partial \phi^{(e)}}{\partial \phi_i}] \, dv^{(e)} + \int_{S_2^{(e)}} (g \frac{\partial \phi^{(e)}}{\partial \phi_i}) \, dS_2 \qquad (18)$$

If Node i does not lie on S_2, the second integral does not appear. Referring to Equation 17, these terms typically become:

$$\begin{cases} \frac{\partial \phi^{(e)}}{\partial x} = \sum_{i=1}^{\gamma} \frac{\partial N_i}{\partial x} \phi_i = [\partial N/\partial x]\{\phi\}^{(e)} \\ \\ \frac{\partial}{\partial \phi} (\frac{\partial \phi^{(e)}}{\partial x}) = \frac{\partial N_i}{\partial x} \\ \\ \frac{\partial \phi^{(e)}}{\partial \phi_i} = N_i \end{cases}$$

Thus on Surface $S_2^{(e)}$ (Equation 14) we have:

$$\frac{\partial I(\phi^{(e)})}{\partial \phi_i} =$$

$$\int_{v^{(e)}} [\mu_x [\partial N/\partial x]\{\phi\} \frac{\partial N_i}{\partial x} + \mu_y [\partial N/\partial y]\{\phi\} \frac{\partial N_i}{\partial y} + \mu_z [\partial N/\partial z]\{\phi\} \frac{\partial N_i}{\partial z} + f N_i] \, dv^{(e)}$$

$$+ \int_{S_2^{(e)}} [g N_i] \, dS_2^{(e)}$$

Let $\phi = -\Sigma N_i \phi_i$, then

$$\begin{Bmatrix} \frac{\partial \phi}{\partial x} = \Sigma \frac{\partial N_i}{\partial x} \phi_i \\ \frac{\partial \phi}{\partial y} = \Sigma \frac{\partial N_i}{\partial y} \phi_i \\ \frac{\partial \phi}{\partial z} = \Sigma \frac{\partial N_i}{\partial z} \phi_i \end{Bmatrix} \tag{19}$$

$$\begin{Bmatrix} \frac{\partial \phi}{\partial x} \\ \frac{\partial \phi}{\partial y} \\ \frac{\partial \phi}{\partial z} \end{Bmatrix} = [B(x, y, z)]\phi_i$$

where

$$[B(x, y, z)] = \begin{bmatrix} \frac{\partial N_1}{\partial x} & \frac{\partial N_2}{\partial x} & \cdots\cdots\cdots & \frac{\partial N_\gamma}{\partial x} \\ \frac{\partial N_1}{\partial y} & \frac{\partial N_2}{\partial y} & \cdots\cdots\cdots & \frac{\partial N_\gamma}{\partial y} \\ \frac{\partial N_1}{\partial z} & \frac{\partial N_2}{\partial z} & \cdots\cdots\cdots & \frac{\partial N_\gamma}{\partial z} \end{bmatrix}$$

From Equation 19, this may be rewritten

$$\int_v [B]^T [k_t][B]\{\phi\}\, dv + \int_v [fN_i]\, dv + \int_{S_2} [gN_i]\, dS_2 = 0 \tag{20}$$

where $\{\phi\} = \begin{Bmatrix} \phi_1 \\ \phi_2 \\ \vdots \\ \phi_\gamma \end{Bmatrix}$ (nodal value)

$$[k_t] = \begin{bmatrix} \mu_x & & 0 \\ & \mu_y & \\ 0 & & \mu_z \end{bmatrix}$$

$[k_t]$ = magnetic permeability on the principal axis (μ_x, μ_y, and μ_z).

2.2.3 Task IIC - Graded Composite Materials

An investigation into the merits of various numerical integration schemes has been pursued in order to determine which schemes might be best suited to the calculation of stiffness matrices for elements composed of several layers of different composite materials. All of the schemes investigated to this point integrate by summing weighted properties evaluated at sampling points which are spaced throughout the element volume. The differences between the various schemes is in the weights associated with the sampling points and the distribution of the sampling points.

The modularization of the stiffness routines allows fairly easy implementation of the various integration schemes. At present, the Gauss integration schemes and Newton-Cotes integration schemes have been coded. In addition, a selective Gauss integration scheme has been coded which uses different Gauss integration orders for calculation of normal stress/strain terms than the order used for shear stress/strain terms. Element stiffness matrices have been obtained using these methods, and a consistent, accurate method for comparing them is being worked on.

The previously coded stiffness routines for the 8-, 16-, and 20-noded isoparametric brick elements have been included in an existing finite-element code, and an extended checkout has begun. Elastic test case runs of isotropic materials have begun with comparisons to an existing finite-element code as well as the critical results.

The test cases run to this point are from "A Proposed Standard Set of Problems to Test Finite Element Accuracy," by R.H. MacNeal and R.L. Harder, a paper presented at the 25th SDM Finite Element Validation Forum, May 14, 1984, and are patch tests and cantilevered-element assemblages for eight-noded-brick elements (Figures 11 - 13). Tables 4 and 5 summarize the results of some of the test cases, and the theoretical results are presented in Table 6. It should be noted that all of these cases were run using single precision. Further improvement in the calculated answers is expected if double precision is used, and this will be investigated in the future.

The 8-noded-brick results show that in the bending test cases the use of incompatible modes produces a considerably better solution as measured by tip displacement of the cantilevered beam model. However, the straightforward inclusion of incompatible modes causes the element to fail the patch test, as can be seen in the result for the existing code. An attempt to rectify this problem was made in the CSTEM code and is reflected in the results. Here,

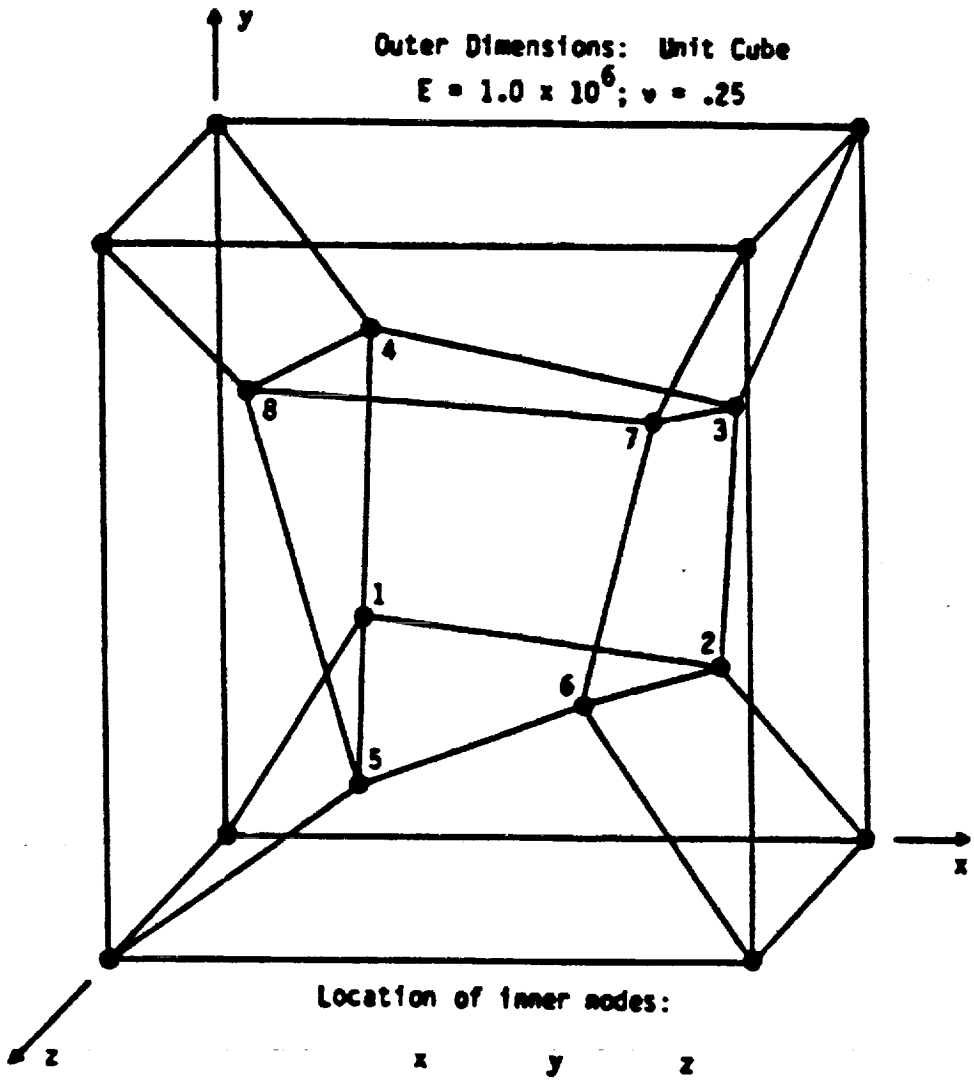

Location of inner nodes:

	x	y	z
1	.249	.342	.192
2	.826	.288	.288
3	.850	.649	.263
4	.273	.750	.230
5	.320	.186	.643
6	.677	.305	.683
7	.788	.693	.644
8	.165	.745	.702

Boundary Conditions: $u = 10^{-3}(2x + y + z)/2$

$v = 10^{-3}(x + 2y + z)/2$

$w = 10^{-3}(x + y + 2z)/2$

Figure 11. Patch Test for Solids.

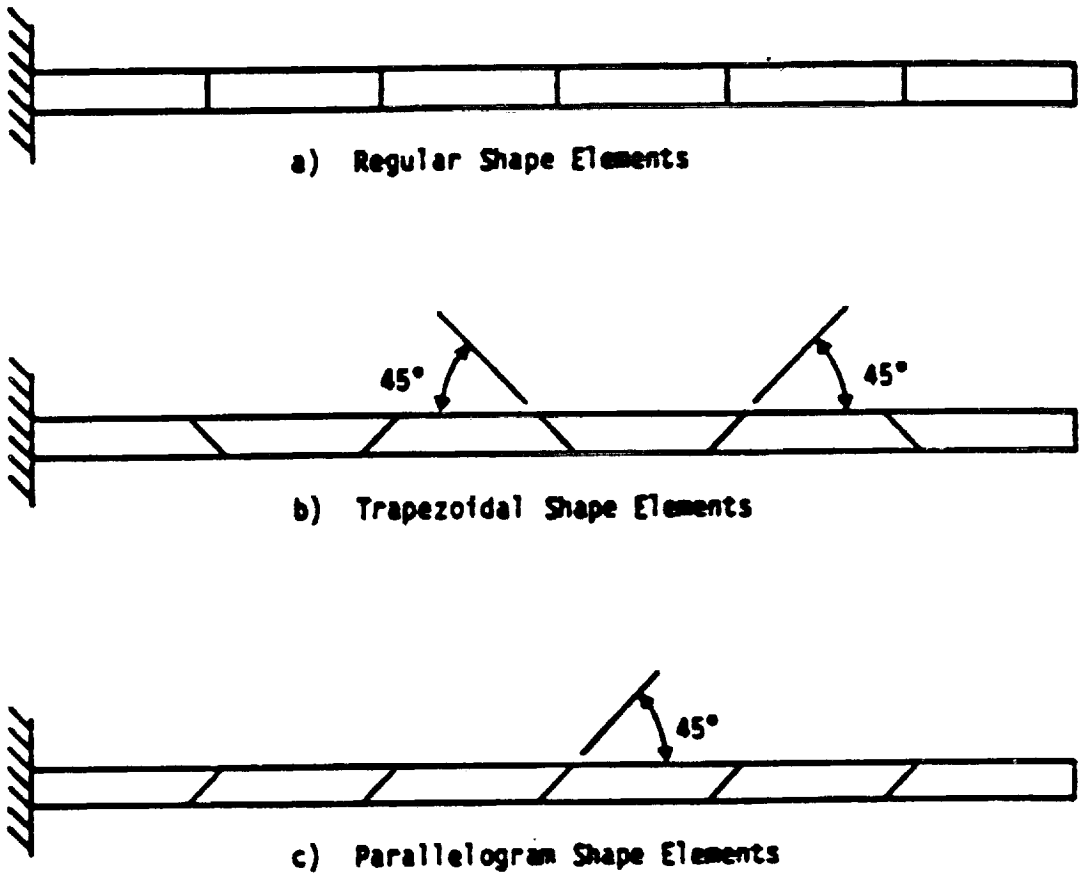

Length = 6.0; Width = 0.2; Depth = 0.1

$E = 1.0 \times 10^{7}$; $\nu = 0.30$; Mesh = 6 x 1

Loading: Unit forces at free end

Note: All elements have equal volume

Figure 12. Straight Cantilever Beam.

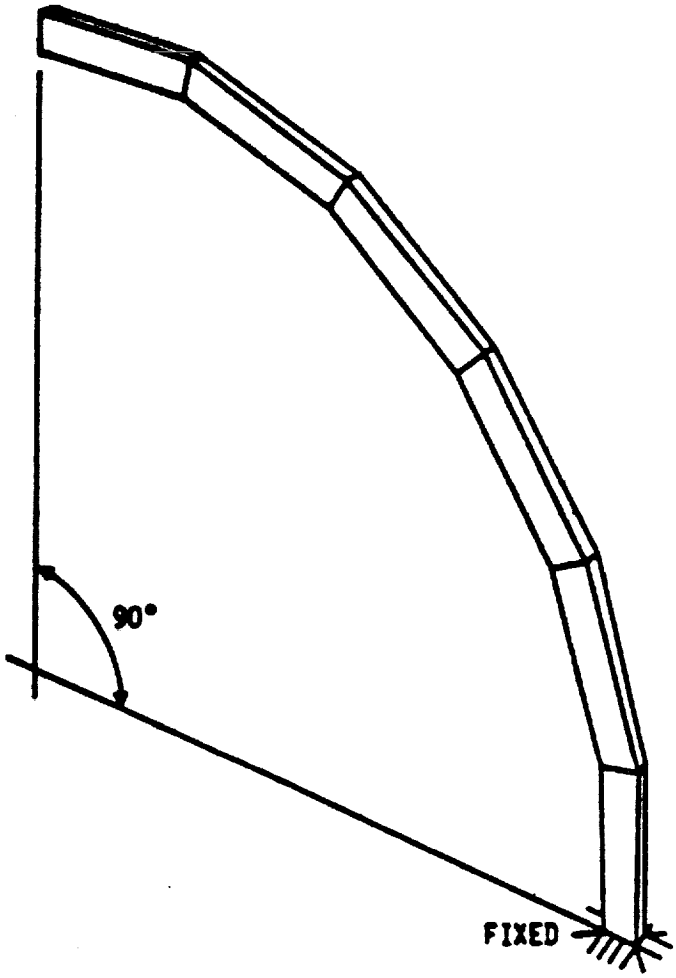

Inner Radius = 4.12; Outer Radius = 4.32; Arc = 90°
Thickness = 0.1; E = 1.0×10^7; ν = 0.25; Mesh = 6 x 1
Loading: Unit forces at tip

Figure 13. Curved Beam.

Table 4. Existing FEM Code.

Eight-Noded Bricks

		Without Incompatibles	With Compatibles
Patch Test		0%	150%
		% Error in Stress	
		Without Incompatibles	With Compatibles
Cantilevered Beam			
Rectangular Elements	Extension	0.9856 (1.4%)	0.9875 (1.2%)
	In Plane	0.0928 (90.7%)	0.9922 (0.8%)
	Out of Plane	0.0252 (97.5%)	1.070 (7.0%)
	Twist	0.8383 (16.2%)	0.7830 (21.7%)
Trapezoid Elements	Extension	0.9845 (1.5%)	1.007 (0.7%)
	In Plane	0.0040 (96.0%)	0.1855 (81.4%)
	Out of Plane	0.0067 (99.3%)	0.0286 (97.1%)
	Twist	0.6075 (39.2%)	0.6507 (34.9%)
Parallelogram Elements	Extension	0.9846 (1.5%)	1.011 (1.1%)
	In Plane	0.0543 (94.6%)	0.7284 (27.2%)
	Out of Plane	0.0084 (99.2%)	0.6367 (36.3%)
	Twist	0.4541 (54.6%)	0.7584 (24.2%)
Curved Beam			
	In Plane	0.0732 (92.7%)	0.9498 (5.0%)
	Out of Plane	0.2249 (77.5%)	0.7874 (21.3%)
		Normalized Tip Displacement (% Error)	

Table 5. CSTEM Stiffness Code.

Eight-Noded Bricks

		Without Incompatibles	With Compatibles
Patch test		0%	0%
		% Error in Stress	
		Without Incompatibles	With Compatibles
Cantilevered Beam			
Rectangular Elements	Extension	0.9856 (1.4%)	0.9875 (1.2%)
	In Plane	0.0928 (90.7%)	0.9922 (1.8%)
	Out of Plane	0.0252 (97.5%)	0.9081 (9.2%)
	Twist	0.8394 (16.1%)	0.8186 (18.1%)
Trapezoid Elements	Extension	0.9845 (1.5%)	1.007 (0.7%)
	In Plane	0.0040 (96.0%)	0.1851 (81.5%)
	Out of Plane	0.0067 (99.3%)	0.0285 (97.1%)
	Twist	0.6078 (39.2%)	0.6502 (35.0%)
Parallelogram Elements	Extension	0.9846 (1.5%)	1.009 (0.9%)
	In Plane	0.0543 (94.6%)	0.7343 (26.6%)
	Out of Plane	0.0084 (99.2%)	0.5960 (40.4%)
	Twist	0.4543 (54.6%)	0.8008 (19.9%)
Curved Beam			
	In Plane	0.0733 (92.6%)	0.9520 (4.8%)
	Out of Plane	0.2265 (77.4%)	0.8771 (12.3%)
		Normalized Tip Displacement (% Error)	

Table 6. Theoretical Solutions.

Patch Test

$\varepsilon x = \varepsilon y + \varepsilon z = \gamma xy = \gamma yz = \gamma zx = 10^{-3}$

$\sigma x = \sigma y = \sigma z = 2000$ psi, $\tau xy = \tau yz = \tau zx = 400$ psi

Straight Beam (Tip Displacement in Direction of Load)

Extension	3.0×10^{-5} in.
In Plane	0.1081 in.
Out of Plane	0.4321 in.
Twist	0.00341 in.

Curved Beam (Tip Displacement in Direction of Load)

In Plane	0.08734 in.
Out of Plane	0.5022 in.

the incompatible modes are included in the stiffness matrix and thus in the solution of the system of equations. This improves displacements; however, the recovery of stress from the displacement solution doesn't include incompatible modes, so the patch test is satisfactory. Along with other possibilities, this technique is still being investigated.

Another observation that can be made is the reinforcement of the fact that modeling technique can greatly influence the results. This is evident from the use of trapezoid- and parallelogram-shaped elements to solve the same cantilever beam problem. A trapezoid-shaped element in particular should be avoided in view of the bad results.

The 20-noded brick passes the patch test with no problem regardless of integration order or whether single or double precision is used. The 20-noded brick is a quadratic displacement element by nature, and so there are no incompatible modes associated with it. The problem with the patch test as exhibited in the 8-noded brick is then avoided by the 20-noded brick.

The regular beam was used for the remainder of the investigation. Because of the single layer of elements, reduced integration produces poor results when looking at displacements. This is due to the presence of zero energy modes: spurious nodal displacements which still satisfy the elemental equations at the Gauss points. More than one layer of elements would help to eliminate this phenomena due to the continuity of the element boundaries.

It was found that the use of single or double precision would greatly affect the results as can be seen in the tabulated results, Table 7. This points to a numerical sensitivity to rounding off or truncation. Using the CSTEM code, attempts were made to improve the results by performing certain operations in double precision while the majority of operations remained in single precision. It was finally found that the best improvement was obtained by calculating the shape functions using double precision while all other operations remained single precision.

2.2.4 Task IID - I/O and Solution Techniques

To achieve computational efficiency and to avoid repeated codings, a modular equation solver has been written to perform combinations of the following functions:

- Matrix decomposition (matrix triangularization)
- Force vector reduction and back-substitution
- Matrix decomposition and force vector back-substitution
- Partial matrix static condensation
- Matrix determinant and Sturm sequence count.

Investigations of the eigenvalue/eigenvector large deformation structural problem were conducted. Two popular techniques were studied: determinant search and subspace iteration.

Table 7. Twenty-Noded Bricks.

EXISTING FEM CODE

	2nd Order	3rd Order	3rd Order Double Prec.	3rd Order Double Prec. Shape
Patch Test (% error in stress)	0	0		
Beam				
Extension	0.9986(0.1%)	0.9941(0.6%)	0.9942(0.6%)	
In Plane	0.3556(64.0%)	0.9950(0.5%)	0.9711(2.9%)	
Out of Plane	-2.23(323%)	1.146(14.6%)	0.9609(3.9%)	
Twist	-0.1187(112%)	0.4305(56.9%)	0.8516(14.8%)	

CSTEM FEM CODE

	2nd Order	3rd Order	3rd Order Double Prec.	3rd Order Double Prec. Shape
Patch Test (% error in stress)	0	0		
Beam				
Extension	0.9988(0.1%)	0.9941(0.6%)	0.9942(0.6%)	0.9942(0.6%)
In Plane	0.2860(71.4%)	0.9946(0.5%)	0.9711(2.9%)	0.9792(2.1%)
Out of Plane	0.3030(69.7%)	0.6043(40.0%)	0.9609(3.9%)	0.9352(6.5%)
Twist	0.5742(42.6%)	0.8406(15.9%)	0.8516(14.8%)	0.5363(46.4%)

Determinant Search - This technique employs inverse iteration in conjunction with eigenshift and Rayleigh quotient method. This method relies heavily on the equations solver to compute Sturm sequence checks and matrix determinants. The starting trial eigenvector plays a very important role in converging to the appropriate corresponding eigenpair. Orthogonality criteria must be imposed for computing repeated, or cluster, eigenpairs.

Subspace Iteration - This method employs inverse iteration, subspace transformation, and Jacoby successive rotation. Besides the efficient equations solver, this method relies heavily on the stiff/mass ratio and convergence criteria. This method will generally compute the desired eigenpairs, but it may not guarantee the lowest eigenpairs.

Constraint equations play a very important role in solving boundary value problems. Two techniques have been developed for solving FEM structural problems with constraints. The first technique is the so-called "penalty function" method which treats the constraint equation as a stiff finite element and is very easy to incorporate in the program, such as:

- To construct a fairly stiff symmetric stiffness matrix out of the given linear constraint equation
- To assemble the constraint stiffness matrix into the global overall structural stiffness matrix.

The technique generally yields satisfactory solutions as long as the number of constraints is not large.

The second technique is the classical matrix partitioning method. For computational efficiency, Gauss elimination is used to perform static condensation rather than using matrix inversion to effect matrix partitioning and reduction. This method is mathematically exact and should be employed when the number of constraints becomes large. However, implementation of this technique into the program may be complicated due to the variation of structural modelings.

For those stress computations within the finite element, Lagrange interpolation demonstrated very good results when data are interpolated or extrapolated from the known Gaussian quadrature quantities.

In order to extend the program capability from static analysis to eigenvalue/eigenvector dynamic analysis, the assembly of consistent mass matrices is required. Because of the similarity between element stiffness matrix and element consistent mass matrix, the assembly routines were extended to accommodate either.

A new data file structure has also been added to the CSTEM stiffness routines. The investigation into different integration techniques emphasized the need to base storage of certain data on the integration point, rather than the element as previously done. This is due to the fact that the number of integration points may vary from element to element, depending on the integration scheme used. The new data-file structure was incorporated into the

code used for the preceding investigations, so installation can be considered complete.

2.2.5 Task IIE - Stand-Alone Codes

These capabilities are being generated as stand-alone codes while the development continues. The major effort in this area is the development of the file structure and data flow for this complex, interconnected problem. A change in the file structure is under consideration as a result of the larger number of integration points being considered. The present element-based file structure will not adequately handle this problem.

APPENDIX A - ACCUMULATED LITERATURE

AEBG Literature Search

1. Allen, D.H., "Predicted Axial Temperature Gradient in a Viscoplastic Uniaxial Bar Due to Thermomechanical Coupling," Texas A&M University, MM 4875-84-15, November 1984.

2. Allen, D.H. and Haisler, W.E., "Predicted Temperature Field in a Thermomechanically Heated Viscoplastic Space Truss Structure," Texas A&M University, MM 4875-85-1, January 1985.

3. Kersch, U., "Approximate Reanalysis for Optimization Along a Line," Int. J. Num. Meth. Engrg., Vol. 18 pp 635-650, 1982.

4. Berger, M.A. and McCullough, R.L., "Characterization and Analysis of the Electrical Properties of a Metal-filled Polymer," Composites Science and Technology, 22, pp 81-106, 1985.

5. McCullough, R.L., "Generalized Combining Rules for Predicting Transport Properties of Composite Materials," Composites Science and Technology, 22, pp 3-21, 1985.

6. Minagawa, S., Nemat-Nasser, S., and Yanada, M., "Dispersion of Waves in Two-Dimensional Layered Fiber-Reinforced, and other Eleastic Composites," Computers and Structures, Vol. 19, No. 1-2, pp 119-128, 1984.

7. Oliver, J. and Onate, E., "A Total LaGrangian Formulation for the Geometrically Nonlinear Analysis of Structures using Finite Elements. Part 1 Two-Dimensional Problems: Shell and Plate Structures," Int. J. Num. Meth. Eng., Vol. 20, pp 2253-2281, 1984.

8. Adams, D.F. and Crane, D.A., "Combined Loading Micro-Mechanical Analysis of a Unidirectional Composite," Composites, Vol. 15, No. 3, pp 181-192, 1984.

9. Ni, R.G. and Adams, R.D., "A Rational Method for Obtaining the Dynamic Mechanical Properties of Laminae for Predicting the Stiffness and Damping of Laminated Plates and Beams," Composites, Vol. 15, No. 3, pp 193-199, 1984.

10. Reddy, J.N. and Chandrosheklara, K., "Nonlinear Analysis of Laminated Shells Including Transverse Shear Strains," AIAA J., Vol. 23, No. 3, pp 440-441, 1985.

11. Pedersen, P. and Jorgensen, L., "Minimum Mass Design of Elastic Frames Subjected to Multiple Load Cases, "Computers and Structures Vol. 18, No. 1, pp 147-157, 1984.

PAGE 78 INTENTIONALLY BLANK

12. Maymon, G., "Response of Geometrically Nonlinear Elastic Structures to Acoustic Excitation - An Engineering Oriented Computational Procedure," Computers and Structures Vol. 18, No. 4, pp 647-652, 1984.

13. Nomura, S. and Chow, T.W., "Bounds for Elastic Moduli of Multiphase Short-Fiber Composites," ASME Journal of Applied Mechanics, Vol. 59, pp 540-545, 1984.

14. Bert, C.W. and Gordaninejad, F., "Forced Vibration of Timoshenco Beams made of Multimodular Materials," ASME Journal of Vibration, Acoustics, Stress, and Reliability in Design, Vol. 107, pp 98-105, 1985.

15. Takenti, Y., Furukawa, T., and Tanigawa, Y., "The Effect of Thermoelastic Coupling for Transient Thermal Stresses in a Composite Cylinder," ASME Journal of Vibration, Acoustics, Stress, and Reliability in Design, Vol. 106, pp 529-532, 1984.

16. Abondi, J. and Benveniste, U., "Constitutive Relations for Fiber-Reinforced Inelastic Laminated Plates," ASME Journal of Applied Mechanics, Vol. 51, pp 107-113, 1984.

17. Wilson, E.L., Taylor, R.L., Doherty, W.P., and Ghabonski, J., Incompatible Displacement Models," Numerical and Computer Methods in Structural Mechanics, Academic Press, 1973.

18. MacNeal, R.H. and Harder, R.L., "A Proposed Standard Set of Problems to Test Finite Element Accuracy," 25th SDM, Finite Element Validation Forum, May 14, 1984.

19. Casey, J.K., Moore, C.L., and Bartlett, J.C., "Automatic Improvement of Design (AID) User's Manual," General Electric R67FPD214, May 1967.

20. Platt, C.E., Pratt, T.K., and Brown, K.W., "Structural Tailoring of Engine Blades (STAEBL)," NASA CR-167949, June 1982.

21. Zienkiewicz, O.C. and Nayak, G.C., "A General Approach to Problems of Large Deformation and Plasticity using Iso-Parametric Elements," 3rd Conference on Matrix Methods in Structural Mechanics, Wright Patterson Air Force Base, October 19-21, 1971.

22. Mondkar, D.P. and Powell, G.H., "3D Solid Element (Type 4 - Elastic or Elastic-Perfectly-Plastic) for the ANSR-II Program," NSF/RA800293, July 1980.

23. Chamis, C.C. and Minich, M.D., "Structural Response of Fiber Composite Fan Blades," ASME 75-GT-78, 1975.

24. Bathe, K.J., Finite Element Procedures in Engineering Analysis, Prentice-Hall, Inc., Englewood Cliffs, New Jersey, 1982.

25. Khot, N.S., "Optimality Criterion Methods in Structural Optimization," AFWAL-TR-81-3124, October 1982.

26 Jense, P.S. and Loden, W.A., "Supplementary Studies on the Sensitivity of Optimized Structures," AFWAL-TR-81-3013, March 1981.

27. Batt, J.R., Gellin, S., and Gellatly, R.A., "Force Method Optimization II, Volume I - Theoretical Development," AFWAL-TR-82-3088 Volume I, November 1982.

28. Batt, J.R., Dale, B.J., Skalski, S.C., Witkop, D.L., and Gellin, S., "Force Method Optimization II, Volume II, User's Manual," AFWAL-TR-82-3088, Volume II, November 1982.

29. Bushnell, D., "Computerized Analysis of Shells - Governing Equations," AFWAL-TR-81-3048, December 1981.

30. Chari, M.V.K., Berkery, K.F., and Ogle, M.D., "Finite Element Evaluation of Power Losses in Electrical Devices of Axisymmetric Cross-Section," General Electric R81CRD168, July 1981.

31. Flanagan, G.V., "Composite Laminate Weight Optimization on the HX-20," AFWAL-TR-83-4061, August 1983.

32. Flanagan, G.V. and Park, W.J., "Composite Laminate Weight Optimization on the Sharp PC-1500 Pocket Computer," AFWAL-TR-83-4095, August 1983.

33. McKnight, R.L., "Poroloy Shroud Analysis," General Electric R73AEG323, 1973.

34. Chang, F.K., Scott, R.A., and Springer, G.S., "Strength of Bolted Joints in Laminate Composites," AFWAL-TR-84-4029, March 1984.

35. Boyd, Harris, King, and Welch, Electronic Countermeasures, Peninsula Publishing, 1978.

36. Emerson and Cuming 1982 Products Catalog.

37. Krueger, C.H., "A Computer Program for Determining the Reflection and Transmission Properties of Multilayered Plane Impedance Boundaries," AFWAL-TR-67-191, September 1967.

Contributed by Texas A&M Consultants

1. Duhamel, J.M.C., "Memoire sur le calcul des actions moleculaires developpees par les changements de temperature dans les corps solides," Memories par divers savans, vol. 5, pp 440-498, 1838.

2. Neuman, F., Vorlesungen uver die Tjeorie der Elasticitat der festen Korper und des Lichtathers, pp 107-120, Leipzig, 1885.

3. Boley, B.A., "Survey of Recent Developments in the Fields of Heat Conduction in Solids and Thermo-Elasticity," Nuclear Ekngineering and Design, Vol. 18, pp 377-399, 1972.

4. Danilovskaya, V.I., "Thermal Stresses in an Elastic Half-Space Arising After a Sudden Heating of its Boundary," Prikl. Mat. Mekh., Vol. 14, pp 316-318, 1950.

5. Danilovskaya, V.I., "On a Dynamic Problem of Thermoelasiticity," Prikl. Mat. Mekh., Vol. 16, pp 341-344, 1952.

6. Boley, B.A. and Weiner, J.H., Theory of Thermal Stresses, Wiley, New York, 1960.

7. Coleman, B.D., "Thermodynamics of Materials with Memory," Archives for Rational Mechanics and Analysis, Vol. 17, pp 1-46, 1964.

8. Takeuti, Y., "Foundations for Coupled Thermoelasticity," Journal of Thermal Stresses, Vol. 2, pp 323-339, 1979.

9. Boley, B.A., "Thermal Stresses Today," source unknown.

10. Bargmann, H., "Recent Developments in the Field of Thermally Induced Waves and Vibrations," Nuclear Engineering and Design, Vol. 27, pp 372-385, 1974.

11. Chester, M., "Second Sound in Solids," Physics Review, Vol. 131, pp 2013-2015, 1963.

12. Biot, M.A., "Thermo-elasticity and Irreversible Thermodynamics," Journal of Applied Physics, Vol. 27, pp 240-251, 1956.

13. Biot, M.A., "New Methods in Heat Flux Analysis with Application to Flight Structures," Journal of Aeronautical Sciences, Vol. 24, pp 857-874, 1957.

14. Zienkiewicz, O.C. and Cheung, Y.K., "Finite Elements in the Solution of Field Problems," The Engineer, Vol. 220, pp 507-527, 1965.

15. Wilson, E.L. and Nickell, R.E., "Application of the Finite Element Method to Heat Conduction Analysis," Nuclear Engineering and Design, Vol. 4, pp 276-286, 1966.

16. Fraeijs de Veubeke, B.M. and Hogge, M.A., "Dual Analysis for Heat Conduction Problems by Finite Elements," International Kournal for Numerical Methods in Engineering, Vol. 5, pp 65-82, 1972.

17. Aguirre-Ramirez, G. and Oden, J.T., "Finite Element Technique Applied to Heat Conduction in Solids with Temperature Dependent Thermal Conductivity," International Journal for Numerical Methods in Engineering, Vol. 7, pp 345-355, 1973.

18. Wilson, E.L., Bathe, K.J., and Peterson, F.E., "Finite Element Analysis of Linear and Nonlinear Heat Transfer," Nuclear Engineering and Design Vol. 29, pp 110-124, 1974.

19. Bruch, J.C. Jr. and Zyvoloski, G., "Transient Two-Dimensional Heat Conduction Problems Solved by the Finite Element Method," International Journal for Numerical Methods in Engineering, Vol. 8, pp 481-494, 1974.

20. Comini, G., Del Guidice, S., Lewis, R.W., and Zienkiewicz, O.C., "Finite Element Solution of Non-linear Heat Conduction Problems with Special Reference to Phase Change," International Journal for Numerical Methods in Engineering, Vol. 8, pp 613-624, 1974.

21. Donea, J., "On the Accuracy of Finite Element Solutions to the Transient Heat-Conduction Equation," International Journal for Numerical Methods in Emgineering, Vol. 8, pp 103-110, 1974.

22. Kohler, W. and Pittr, J., "Calculation of Transient Temperature Fields with Finite Elements in Space and Time Dimensions," International Journal for Numerical Methods in Engineering, Vol. 8, pp 625-631, 1974.

23. Wood, W.L. and Lewis, R.W., "A Comparison of Time Marching Schemes for the Transient Heat Conduction Equation," International Journal for Numerical Methods in Engineering, Vol. 9, pp 679-689, 1975.

24. Hughes, T.J.R., "Stability of One-Step Methods in Transient Nonlinear Heat Conduction," Transactions of the 4th International Journal for Numerical Methods in Engineering, Vol. 9, pp 679-689, 1975.

25. Bathe, K.J. and Khoshgoftaar, R., "Finite Element Formulation and Solution of Nonlinear Heat Transfer," Nuclear Engineering and Design, Vol. 51, pp 389-401, 1979.

26. Hogge, M.A., "Secant Versus Tangent Methods in Nonlinear Heat Transfer Analysis," International Journal for Numerical Methods in Engineering, Vol. 16, pp 51-64, 1980.

27. Chung, K.S., "The Fourth-Dimension Concept in the Finite Element Analysis of Transient Heat Transfer Problems," International Journal for Numerical Methods in Engineering, Vol. 17, pp 325-325, 1981.

28 Parkus, H., "Methods of Solution of Thermoelastic Boundary Value Problems in High Temperature Structures and Materials," Proceedings of the Third Symposium on Naval Structural Mechanics, 1964.

29. Lord, H.W. and Shulman, Y., "A Generalized Dunamical Theory of Thermoelasticity," Journal of Mechanics and Physics of Solids, Vol. 15, pp 299-309, 1967.

30. Achenbach, J.D., "The Influence of Heat Conduction on Propagating Stress Jumps," Journal of Mechanics and Physics of Solids, Vol. 16, pp 273-282, 1968.

31. Oden, J.T., "Finite Element Analysis of Nonlinear Problems in the Dynamical Theory of Coupled Thermoelasticity," Nuclear Engineering and Design, Vol. 10, pp 465-475, 1969.

32. Oden, J.T. and Kross, D.A., "Analysis of General Coupled Thermoelasticity Problems by the Finite Element Method," Proceedings 2nd Conference on Matrix Methods in Structural Mechanics, AFFDL-TR-68-150, pp 1091-1120, 1969.

33. Oden, J.T., Chung, T.J., and Key, J.E., "Analysis of Nonlinear Thermoelastic and Thermoplastic Behavior of Solids of Revolution by the Finite Element Method," Proceedings 1st International Conference on Structural Mechanics and Reactor Technology, Berlin, 1971.

34. Allen, D.J. and Milly, T.M., "A Comparison of Constitutive Models for Nonlinear Rate Dependent Material Behavior of Solids," Virginia Polytechnic Institute and State University, Report No. VPI-E-81-16, 1981.

35. Burnett, J.A. and Padovan, J., "Residual Stress Fields in Heat-Treated Case-Hardened Cylinders," Journal of Thermal Stresses, Vol. 2, pp 251-263, 1979.

36. Cernocky, E.P. and Krempl, E., "A Coupled, Isotropic Theory of Thermoviscoplasticity Based on Total Strain and Overstress and its Predictions in Monotonic Torsional Loadings, "Journal of Thermal Stresses, Vol. 4, pp 69-82, 1981.

37. Inoue, T., Nagaki, S., and Kawate, T., "Successive Deformation of a Viscoelastic-Plastic Tube Subjected to Internal Pressure under Temperature Cycling," Journal of Thermal Stresses, Vol. 3, pp 185-198, 1980.

38. Huang, S. and Cozzarelli, F.A., "Some Analytical and Numerical Results for Cladded Fuel Rods Subjected to Thermoirradiation Induced Creep," State University of New York at Buffalo, No. 105, 1979.

39. Cernocky, E.P. and Krempl, E., "A Theory of Thermoviscoplasticity Based on Infinitesimal Total Strain," International Journal of Solids and Structures, Vol. 16, pp 723-741, 1980.

40. Mukherjee, S., Kumar, V., and Kuang, J.C., "Elevated Temperature Inelastic Analysis of Metallic Media Under Time Varying Loads Using State Variable Theories," International Journal of Solids and Structures, Vol. 14, pp 663-679, 1978.

41. Perzyna, P., "Fundamental Problems in Viscoplasticity," Advan. Appl. Mech. Vol. 9, pp 243-377, 1966.

42. Zienkiewicz, O.C and Courmeau, I.C., "Visco-Plasticity--Plasticity and Vreep in Elastic Solids--A Unified Numerical Approach," International Journal for Numerical Methods in Engineering, Vol. 8, pp 821-845, 1974.

43. Lee, D. and F. Zaverl, Jr., "A Generalized Strain Rate Dependent Constitutive Equation for Anistropic Metals," Acta. Met., Vol. 26, No. 11, p 1171, 1978.

44. Pugh, C.E., Corum, J.M., Lin, K.C., and Greenstreet, W.L., "Currently Recommended Constitutive Equations for Inelastic Design Analysis of FFTF Components," ORNL TM-3602, Oak Ridge National Laboratory, September 1972.

45. Valanis, K.D., "A Theory of Viscoplasticity Without a Yield Surface, Part I - General Theory," Archives of Mechanics, Vol. 23, pp 517-533, 1971.

46. Laflen, J.H. and D.C. Stouffer, "An Analysis of High Temperature Metal Creep: Part I - Experimental Definition of an Alloy and Part II - A Constitutive Formulation and Verification," ASME J. Eng. Mat. & Tech. 100, p 363, 1978.

47. Walker, K.P., "Representation of Hastelloy-X Behavior at Elevated Temperature with a Functional Theory of Viscoplasticity," presented at ASME Pressure Vessels Conference, San Francisco, Aug. 12, 1980 (Also to appear in ASME Journal of Engineering Materials and Technology).

48. Hart, E.W., "Constitutive Relations for the Nonelastic Deformation of Metals," ASME J. Eng. Mat. & Tech. 98-H, p 193, 1976.

49. Krieg, R.D., Swearengen, J.C., and Rohde, R.W., "A Phsically-Based Internal Variable Model for Rate-Dependent Plasticity," Proceedings ASME/CSME PVP Conference, pp 15-27, 1978.

50. Bodner, S.R. and Partom, Y., "Constitutive Equations for Elastic-Viscoplastic train-Hardening Materials," Journal of Applied Mechanics, Vol. 42, No. 2, pp 385-389, 1975.

51. Miller, A.K., "An Inelastic Constitutive Model for Monotonic, Cyclic, and Creep Deformation: Part I - Equations Development and Analytical Procedures and Part II - Application to Type 304 Stainless Steel," ASME J. Eng. Mat. & Tech. 98-H, p 97, 1976.

52. Lou, Y.C. and Schapery, R.A., "Viscoelastic Characterization of a Nonlinear Fiber-Reinforced Plastic," Journal of Composite Materials, Vol. 5, pp 208-234, 1971.

53. Schapery, R.A., "A Theory of Non-Linear Thermovisco-elasticity Based on Irreversible Thermodynamics," Proceedings 5th U.S. National Congress on Applied Mechanics, pp 511-530, 1966.

54. Schapery, R.A., "On a Thermodynamic Constitutive Theory and Its Application to Various Nonlinear Materials," Proceedings IUTAM Symposium, pp 259-285, 1968.

55. Bouc, R. and Geymonat, G., "Linearized Thermoviscoelasticity with High Temperature Variations and Related Periodic Problems," International Journal of Engineering Science, Vol. 16, pp 681-705, 1978.

56. Frutiger, R.L. and Woo, T.C., "A Thermoviscoelastic Analysis for Circular Plates of Thermorheologically Simple Material," Journal of Thermal Stresses, Vol. 2, pp 45-60, 1979.

57. Herrman, K. and Mattheck, C., "Thermal Stresses in the Unit Cell of a Fiber-Reinforced Material," Journal of Thermal Stresses, Vol. 2, pp 179-191, 1963.

58. Gurtin, M.E., "Variational Principles in the Linear Theory of Viscoelasticity," Archive for Rational Mechanics and Analysis, Vol. 3, pp 179-191, 1963.

59. Leitman, M.J., "Variational Principles in the Linear Theory of Viscoelasticity," Archive for Rational Mechanics and Analysis, Vol. 3, pp 179-191, 1963.

60. Reddy, J.N., "Modified Gurtin's Variational Principles in the Linear Dynamic Theory of Viscoelasticity," International Journal of Solids and Structures, Vol. 12, pp 227-235, 1976.

61. Zienkiewicz, O.C. and Godbole, P.N., "Flow of Plastic and Visco-Plastic Solids with Special Reference to Extension and Forming Processes," International Journal for Numerical Methods in Engineering, Vol. 8, pp 3-16, 1974.

62. Williams, J.R., Lewis, R.W., and Morgan, K., "An Elasto-Viscoplastic Thermal Stress Model with Applications to the Continuous Casting of Metals," International Journal for Numerical Methods in Engineering, Vol. 14, pp 1-9, 1979.

63. Sprinatha, H.R. and Lewis, R.W., "A Finite Element Method for Thermoviscoelastic Analysis of Plane Problems," Computer Methods in Applied Mechanics and Engineering, Vol. 25, pp 21-33, 1981.

64. Allen, D.H. and Haisler, W.E., "A Theory for Analysis of thermoplastic Materials," Computers & Structures, Vol. 13, pp 124-135, 1981.

65. Yamada, Y., "Constitutive Modelling of Inelastic Behavior and Numerical Solution of Nonlinear Problems by the Finite Element Method," Computers & Structures, Vol. 8, pp 533-543, 1978.

66. Snyder, M.D. and Bathe, K.J., "Formulation and Numerical Solution of Thermo-Elastic-Plastic and Creep Problems," National Technical Information Service, No. 82448-3, 1977.

67. Newman, J.B., Giovengo, J.F., and Comden, L.P., "The CYGRO-4 Fuel Rod Analysis Computer Program," Transactions of the 4th International Conference on Structural Mechanics in Reactor Technologu, D 1/1, 1977.

68. Kulak, R.F., Belytschko, T.B., Kennedy, T.M., and Schoeberle, D.F., "Finite Element Formulations for the Thermal Stress Analysis of Two-

and Three-Dimensional Thin Reactor Structures," Transactions of the 4th International Conference on Structural Mechanics in Reactor Technology, E 3/3, 1977.

69. Kulak, R.F. and Kennedy, J.M., "Structural Response of Fast Reactor Core Subassemblies to Thermal Loading," 3rd International Conference on Structural Mechanics in Reactor Technology, E 1/6, 1975.

70. Spaas, H.A.C.M., Mjuazono, S., Kodaira, T., and Ito, K., "Theoretical and Experimental Analysis of Sodium Cooled Nuclear Reactor Nozzle Loaded by Thermal Shocks," 3rd International Conference on Structural Mechanics in Reactor Technology, G 1/5, 1975.

71. Gülkan, P. and Akay, H.U., "Analysis of Prestressed Concrete Reactor Vessels under High Thermal Gradient," 3rd International Conference on Structural Mechanics in Reactor Technology, H 2/4, 1975.

72. Cost, T.L. and Heard, J.M., "Finite-Element Analysis of Coupled Thermo-viscoelastic Structures Undergoing Sustained Periodic Vibrations," AIAA Journal, Vol. 16, pp 795-799, 1978.

73. Truesdell, C. and Toupin, R., "The Classical Field Theories," Encyclopedia of Physics, Vol. III/I, 1960.

74. Truesdell, C. and Noll, W., "The Nonlinear Field Theories of Mechanics," Encyclopedia of Physics, Vol. III/3, 1965.

75. Coleman, B.D. and Noll, W., "The Thermodynamics of Elastic Materials with Heat Conduction and Viscosity," Archive for Rational Mechanics Analysis, Vol. 13, pp 167-178, 1963.

76. Kuznetsov, V.N., Ogibalov, P.M., and Pobedrya, B.E., "The Coupling Problem in Polymer Mechanics," Mikhanika Polimerov, Vol. 1, pp 59-65, 1971.

77. Bykov, D.L., Il'yushin, A.A., Ogibalov, P.M., and Pobedrya, B.E., "Some Fundamental Problems of the Theory of Thermoviscoelasticity," Mikhanika Polimerov, Vol. 1, pp 41-58, 1971.

78. Kovalenko, A.D. and Karnaukhov, V.G., "A Linearized Theory of Thermo-viscoelasticity," Mekhanika Polimerov, Vol. 2, pp 214-221, 1972.

79. Navarro, C.B., "Asympototic Stability in Linear Thermoviscoelasticity," Journal of Mathematical Analysis and Applications, Vol. 65, pp 399-431, 1978.

80. Chang, W.P. and Cozzarelli, F.A., "On the Thermodynamics of Nonlinear Single Integral Representations for Thermoviscoelastic Materials with Applications to One-Dimensional Wave Propagation," Acta Mechanica, Vol. 25, pp 187-206, 1977.

81. Lee, C., Chang, W.P., and Cozzarelli, F.A., "Some Results on the One-Dimensional Coupled Nonlinear Thermoviscoelastic Wave Propagation Problem with Second Sound," Acta Mechanica, Vol. 37, pp 111-129, 1980.

82. Turkan, D. and Mengi, Y., "The Propagation of Discontinuities in Non-Homogeneous Thermoviscoelastic Media," Journal of Sound and Vibration, Vol. 70, pp 167-180, 1980.

83. Nunziato, J.W. and Walsh, E.K., "Amplitude Behavior of Shock Waves in a Thermoviscoelastic Solid," International Journal of Solids and Structures, Vol. 15, pp 513-517, 1979.

84. Young, R.W., "Sensitivity of Thermomechanical Response to Thermal Boundary Conditions and Material Constants," International Journal of Solids and Structures, Vol. 15, pp 513-517, 1979.

85. Ting, E.C. and Tuan, J.L., "Effect of Cyclic Internal Pressure on the Temperature Distribution in a Viscoelastic Cylinder," International Journal of Mechanical Sciences, Vol. 15, pp 861-871, 1973.

86. Young, R.W., "Thermomechanical Response of aViscoelastic Rod Driven by a Sinusoidal Displacement," International Journal of Solids and Structures, Vol. 13, pp 925-936, 1977.

87. Mukherjee, S., "Variational Principles in Dynamic Thermoviscoelasticity," International Journal of Solids and Structures, Vol. 9, pp 1301-1316, 1973.

88. Reddy, J.N., "Variational Principles in Dynamic Thermoviscoelasticity," International Journal of Solids and Structures, Vol. 9, pp 1301-1316, 1973.

89. Reddy, J.N., "A Note on Mixed Variational Principles for Initial-Value Problems," Quarterly Journal of Mechanics and Applied Mathematics, Vol. 28, 1975.

90. Oden, J.T. and Reddy, J.N., Variational Methods in Theoretical Mechanics, Springer-Verlag, New York, 1976.

91. Batra, R.C., "Cold Sheet Rolling, The Thermoviscoelastic Problem, A Numerical Solution," International Journal for Numerical Methods in Engineering, Vol. 11, pp 671-682, 1977.

92. Batra, R.D., Levinson, M., and Betz, E., "Rubber Covered Rolls - The Thermoviscoelastic Problem. A Finite Element Solution," International Journal for Numerical Methods in Engineering, Vol. 10, pp 767-785, 1976.

93. Oden, J.T., "Finite Element Approximations in Nonlinear Thermoviscoelasticity," NATO Advanced Study Institute on Finite Element Methods in Continuum Mechanics, Lisbon, 1971.

94. Oden, J.T., Finite Elements of Nonlinear Continua, McGraw-Hill, New York, 1972.

95. Oden, J.T., Bhandari, D.R., Yagawa, G., and Chung, T.J., "A New Approach to the Finite-Element Formulation and Solution of a Class of Problems in Coupled Thermoelastoviscoplasticity of Crystalline Solids," Nuclear Engineering and Design, Vol. 24, pp 420-430, 1973.

96. Strang, G. and Matthies, H., "Numerical Computations in Nonlinear Mechanics," presented at the Pressure Vessels and Piping Conference, ASME, No. 79-PVP-103, San Francisco, 1979.

97. Allen, D.H., "Predicted Axial Temperature Gradient in a Viscoplastic Uniaxial Bar Due to Thermomechanical Coupling," Texas A&M University, MM 4875-84-15, November 1984.

98 Allen, D.H., and Haisler, W.E., "Predicted Temperature Field in a Thermomechanically Heated Viscoplastic Space Truss Structure," Texas A&M University, MM 4875-85-1, January 1985.

APPENDIX B - EIGENVALUE SOLUTIONS

Closed-form eigenvalue solutions of cantilever continuous beam with rectangular cross section

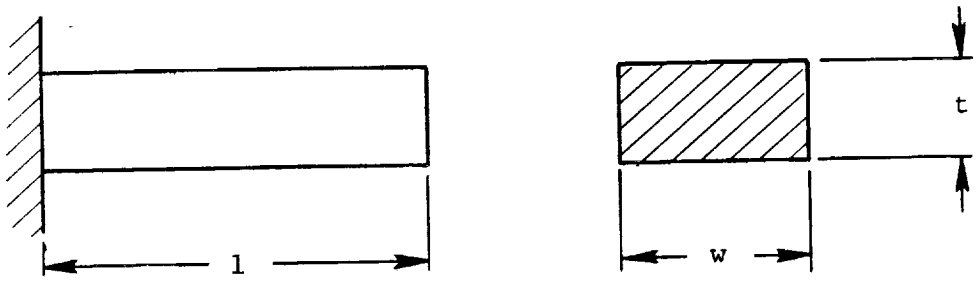

$$\lambda_i \equiv W_i^2 = \left(\frac{\alpha_i}{L}\right)^4 \frac{EI}{\gamma}$$

where

E = Young's modulus

I = Area moment of inertia = $wt^3/12$

λ = Mass per unit length = ρwt

ρ = Mass density

α_i = Constants = 1.875, 4.694, 7.855, ...

Finite Element Models and Results

1. Four MSS8 shell elements of equal length were used.

2. Material data:

   $E = 30 \times 10^6$ psi

   $\rho = 0.298/386 \ \frac{\text{lb-sec}^2}{\text{in}^4}$

3. Constant cantilever dimensions:

   L = 8 in.

   W = 2 in.

4. Results:

Test Case Thickness	Theoretical	MSS8
t = 2 in.	$\lambda_1 = 39$	$\lambda_1 = 38.9$
	$\lambda_2 = 1535$	$\lambda_2 = 1014$
t = 1 in.	$\lambda_1 = 9.77$	$\lambda_1 = 10.3$
	$\lambda_2 = 384$	$\lambda_2 = 347$
t = 0.2 in.	$\lambda_1 = 0.39$	$\lambda_1 = 0.42$
	$\lambda_2 = 15.4$	$\lambda_2 = 15.7$
	$\lambda_3 = 120$	$\lambda_3 = 118$

APPENDIX C - EIGENSHIFT AND RAYLEIGH QUOTIENT EXAMPLE

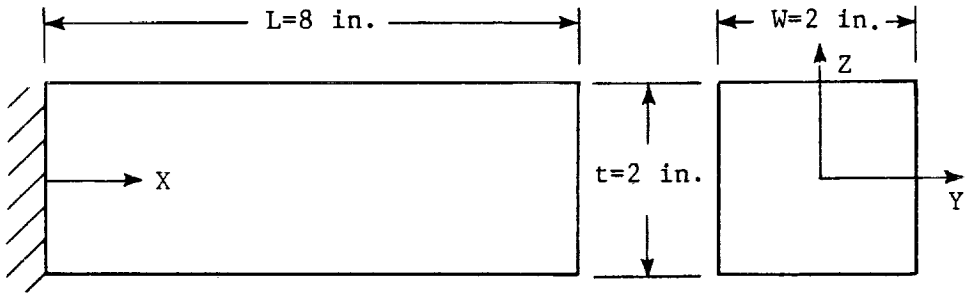

$E = 30 \times 10^6$ psi, $\nu = 0.3$, $\rho = 0.298 \times 10^8$ lb/in^3

Mode Shape (Axis-About)	Eigen Values	
	Subspace Iterations	Eigenvalue Shift and Rayleigh Quotient
1st $Bend_E$	0.357145302	0.3 + 0.057320891
1st $Bend_Y$	0.362975676	0.4 - 0.037155197
1st $Tors_X$	6.24068457	6.0 + 0.24067101
2nd $Bend_Z$		8.0 + 0.79694164
2nd $Bend_Y$	9.53097761	10.0 - 0.46902631
1st $Axial_X$		16.0 - 0.98479339
3rd $Bend_E$		44 + 0.82830848
3rd $Bend_Y$	49.4069934	49 + 0.40698682

REPORT DOCUMENTATION PAGE

Form Approved
OMB No. 0704-0188

1. AGENCY USE ONLY (*Leave blank*)	2. REPORT DATE	3. REPORT TYPE AND DATES COVERED
	April 1992	Final Contractor Report

4. TITLE AND SUBTITLE
Coupled Structural/Thermal/Electromagnetic Analysis/Tailoring of Graded Composite Structures
First Annual Status Report

5. FUNDING NUMBERS
WU–505–62–91
C–NAS3–24538

6. AUTHOR(S)
R.L. McKnight, P.C. Chen, L.T. Dame, H. Huang, and M. Hartle

7. PERFORMING ORGANIZATION NAME(S) AND ADDRESS(ES)
General Electric
Aircraft Engine Business Group
Cincinnati, Ohio 45215

8. PERFORMING ORGANIZATION REPORT NUMBER
None

9. SPONSORING/MONITORING AGENCY NAMES(S) AND ADDRESS(ES)
National Aeronautics and Space Administration
Lewis Research Center
Cleveland, Ohio 44135–3191

10. SPONSORING/MONITORING AGENCY REPORT NUMBER
NASA CR–189150

11. SUPPLEMENTARY NOTES
Project Manager, C.C. Chamis, Structures Division, NASA Lewis Research Center, (216) 433–3252.

12a. DISTRIBUTION/AVAILABILITY STATEMENT
Unclassified - Unlimited
Subject Category 39

12b. DISTRIBUTION CODE

13. ABSTRACT (*Maximum 200 words*)

Accomplishments are described for the first year effort of a 5-year program to develop a methodology for coupled structural/thermal/electromagnetic analysis/tailoring of graded composite structures. These accomplishments include: (1) the results of the selective literature survey; (2) 8-, 16-, and 20-noded isoparametric plate and shell elements; (3) large deformation structural analysis; (4) Eigenanalysis; (5) anisotropic heat transfer analysis; and (6) anisotropic electromagnetic analysis.

14. SUBJECT TERMS
Literature survey; Solid elements; Plate elements; Large deformation; Eigenanalysis; Anisotropic; Heat transfer; Electromagnetic analysis; Graded composites

15. NUMBER OF PAGES
102

16. PRICE CODE
A06

17. SECURITY CLASSIFICATION OF REPORT	18. SECURITY CLASSIFICATION OF THIS PAGE	19. SECURITY CLASSIFICATION OF ABSTRACT	20. LIMITATION OF ABSTRACT
Unclassified	Unclassified	Unclassified	

NSN 7540-01-280-5500

U.S. GOVERNMENT PRINTING OFFICE: 1992 - 750-034/60307

Standard Form 298 (Rev. 2-89)
Prescribed by ANSI Std. Z39-18
298-102